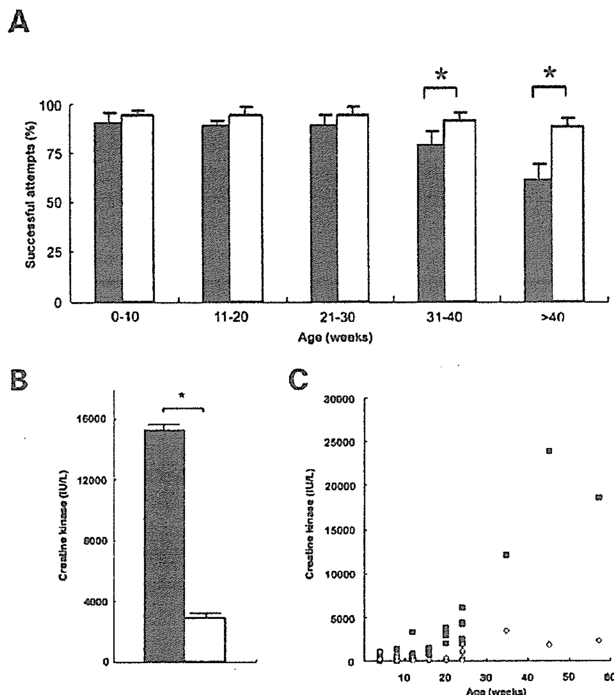

Figure 5. (A) Evaluation of over-all motor strength using rod-climbing test, according to age group. Mean of three trials are shown. *Gne*$^{(-/-)}$ h*GNE*V572L-Tg mice (closed bars, $n = 10$) perform worse than littermates ($n = 10$). Significant difference is noticeable after 30 weeks of age. Asterisk, $P < 0.05$ (Mann–Whitney U test). (B) Measurement of CK activity. Serum CK is significantly higher in *Gne*$^{(-/-)}$h*GNE*V572L-Tg mice (closed bars) when compared with littermates (open bars). Asterisk, $P < 0.05$ (Student's t-test, two-tailed). (C) CK activity according to age. CK activity of *Gne*$^{(-/-)}$ h*GNE*V572L-Tg mice (closed squares) starts to elevate after 30 weeks of age when compared with littermates (open diamonds).

Various proteins are expressed in the *Gne*$^{(-/-)}$h*GNE*V572L-Tg muscles

One of the defining hallmark features of DMRV/h-IBM is the presence of inclusion bodies that are presumed to have a role in muscle degeneration. These deposits have been shown to be immunoreactive to several proteins. Similar to human cases of DMRV, muscle cross sections obtained from the *Gne*$^{(-/-)}$ h*GNE*V572L-Tg mice reveal positive Congo red staining (Fig. 7D), which is not observed in the myofibers of control mice (data not shown). Intense, demarcated signals are seen within the area of RVs and more frequently co-localizing with inclusion bodies which are often seen in DMRV/ h-IBM. As congophilia denotes deposition of proteins assuming a beta-pleated structure, we used the well-characterized 6E10, Aβ1–42, Aβ1–40 and A11 (amyloid β-oligomer), and β-site amyloid precursor protein cleaving enzyme (BACE2) antibodies to check for intracellular accumulation of amyloid. Amyloid depositions occur within the myofibers, and are seen to be occasionally associated with vacuolated fibers, as ~62% of RVs are positive for amyloid expression (data not shown). These amyloid inclusions are also noted in non-vacuolated fibers, including those which appear normal. Amyloid β precursor protein (AβPP), which is recognized by 6E10 antibody (Fig. 7I) has intense, large, fairly demarcated immunoreactive signals within the RVs, similar to the staining pattern of the fibrillar forms of amyloid β or amyloid β peptides 1–42 and 1–40 (Fig. 7J and K). In good agreement with finding amyloid deposits in the myofibers, BACE2, which purportedly represents β-secretase activity, is upregulated in these myofibers and are seen as granular staining in the cytoplasm and intense immunoreactivity at subsarcolemmal areas (Fig. 7H). Interestingly, the oligomer form of amyloid β, which is recognized by A11, is also expressed in the myofibers; positive signals are seen as aggregates around the RVs which are localized in areas distinct from fibrillar forms of amyloid (Fig. 7L).

We then analyzed skeletal muscles of mice from different age groups to see whether these amyloid accumulations are related to or can be considered as a function of age. We found out that these accumulations start to occur from 32 to 34 weeks of age, a period when virtually no RV is seen in the myofibers, and muscle pathology is characterized mainly by mild variation in fiber size (Fig. 8A and C). Both AβPP (Fig. 8B) and amyloid β 1–42 peptide (Fig. 8D) show positive immunoreactivity within the myofibers.

The microtubule-associated protein tau, a cytoskeletal protein, has been shown to be abnormally phosphorylated and accumulated in DMRV and other muscle disorders (21–23). Similarly, in these mice, these deposits are evident as squiggly inclusions which are occasionally seen in vacuolated fibers (Fig. 7M).

SM-31, an antibody which detects neurofilaments, has been well-characterized in DMRV/h-IBM (21,24). In muscle sections, positive staining is seen within the vicinity of RVs (Fig. 7N); not all RVs, however, show immunoreactivity with this antibody. SM-310, on the other hand, only stains the intramuscular nerve bundles (Fig. 7O).

Because of the accumulation of several proteins in the myofibers, ER stress and the unfolded protein response (UPR) have been implicated in the pathogenesis of DMRV/h-IBM. Using an antibody which recognizes one of the ER chaperones, we show that the UPR activation occurs in the *Gne*$^{(-/-)}$ h*GNE*V572L-Tg mice. Intracellular Grp-94 immunoreactivity is seen exclusively in vacuolated fibers (Fig. 7P). In the myofibers of the mice, strong reactivity to ubiquitin antibody in vacuolated and non-vacuolated fibers are seen (Fig. 7Q), suggesting that the ubiquitin–proteosome system may as well be involved in the degradation of abnormal protein accumulations in the muscle, and that misfolded proteins are ubiquitinated but not degraded.

Sarcolemmal proteins are also accumulated in DMRV/ h-IBM myofibers. Within the vicinity of the RVs, positive α-dystroglycan (Fig. 7R), β-dystroglycan (Fig. 7S) and α-sarcoglycan (Fig. 7T) signals are observed.

In the myofibers of the control mice, no protein depositions were appreciated (data not shown).

Electron microscopic studies show evidence of autophagy and inclusions in the *Gne*$^{(-/-)}$h*GNE*V572L-Tg muscles

Ultrastructural studies confirm the activation of autophagy in *Gne*$^{(-/-)}$h*GNE*V572L-Tg muscles (Fig. 9). We obtained samples from a 42-week-old female mouse which had RVs

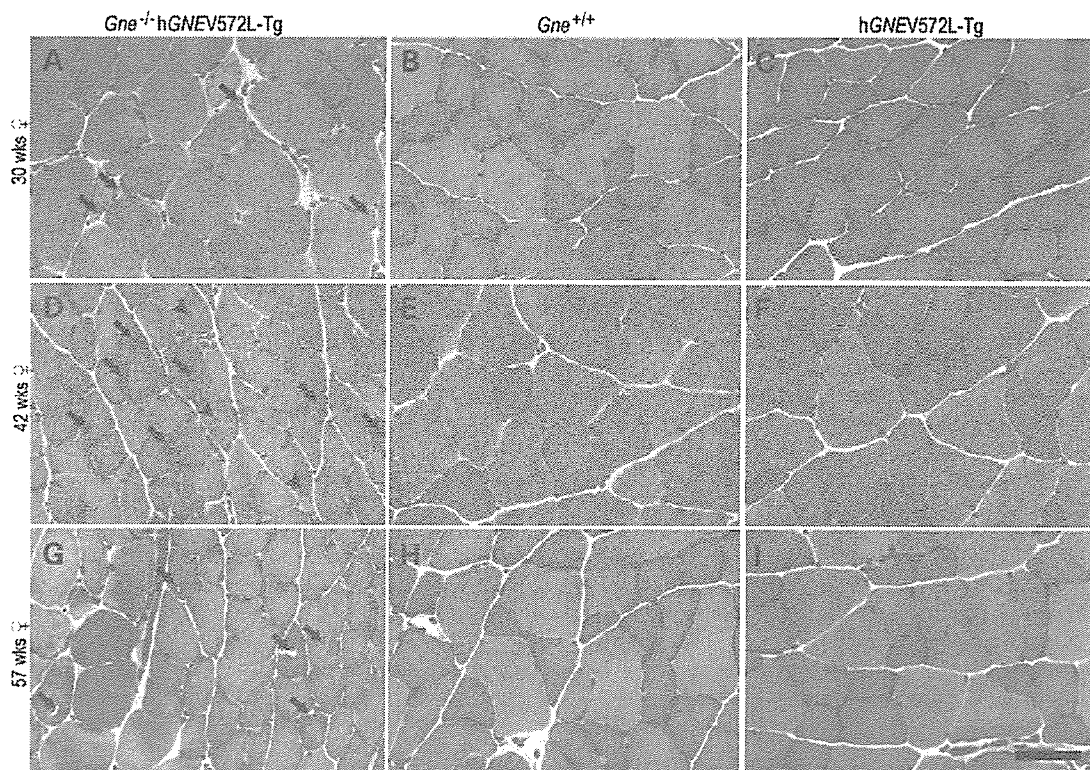

Figure 6. Hematoxylin and eosin sections from *Gne*$^{(-/-)}$h*GNE*V572L-Tg (**A, D, G**), WT (**B, E, H**), h*GNE*V572L-Tg (**C, F, I**). The h*GNE*V572L-Tg mice are comparable with WT in all ages. In the *Gne*$^{(-/-)}$h*GNE*V572L-Tg, there is variation in fiber size which becomes more obvious as the mice age. Fibrosis, necrotic or regenerating processes are not noted. Internalized nuclei are noted in scattered fibers. Small angular fibers are noted from around 30 weeks of age (A, arrows). Fibers with RVs (arrows), as well as cytoplasmic inclusions (arrowhead) are observed in scattered fibers from 42 weeks of age (D and G). Bar represents 40 μm.

as seen in light microscopy. In these samples, disorganization of myofibrils was seen in the vicinity of RVs. In about 500 myofibers examined, 10% showed ultrastructural evidence of autophagy. Collections of lysosomal autophagosomes containing undigested intracellular debris were seen, usually enclosed by a limiting membrane (Fig. 9A, arrow). The debris are often composed of light or electron-dense amorphous materials, and appeared like myelin whorls. Multiple small double membrane-bound autophagic vacuoles were often contained within a larger autophagic vesicle (AV), suggesting that autophagy in these myofibers involves a continual process of AV consolidation (Fig. 9A, arrowhead). Multilamellar bodies are also observed (Fig. 9A, double arrows). Probable amyloid deposits are seen as amorphous and granular material (Fig. 9B, magnified from A). Interestingly, ovoid and densely granular deposits, which may also be amyloid-like structures, are noted not only in the areas of autophagy (Fig. 9A, asterisk), but also in areas where myofibrillar architecture is well preserved (Fig. 9C). Occasionally, autophagic vacuoles are seen within the substance of these deposits (Fig. 9C, arrow).

Gne$^{(-/-)}$h*GNE*V572L-Tg shows pathological changes in the diaphragm and cardiac muscles

It has been a well-accepted fact that DMRV/h-IBM primarily involved the skeletal muscles, and that respiratory muscles are assumed to be spared as there had been no reports implying the involvement of the respiratory system. Interestingly, in the *Gne*$^{(-/-)}$h*GNE*V572L-Tg mice, we found that even diaphragm muscles are involved, although the findings range from almost normal findings to the presence of marked fibrosis and RVs in the myofibers (Fig. 10A). Likewise, we have observed inclusion bodies which are seen in both vacuolated and non-vacuolated fibers (data not shown).

It is now being recognized that some patients manifest with a variety of cardiac abnormalities, from the seemingly benign right bundle branch block to fatal arrhythmias. This led us to carefully check the status of cardiac muscles in the mice. We found out that few mice (around 20%) develop fibrosis in the cardiac tissue after the age of 30 weeks, and some show marked endomysial fibrosis (Fig. 10B). Moreover, amyloid deposition (Fig. 10C) and, occasionally, RVs (Fig. 10D) are also observed in cardiomyocytes. We also tried to functionally evaluate the heart using 2D echocardiography and electrocardiogram, but we did not observe any abnormality pointing to definite cardiomyopathy or conduction defects (data not shown), although we only tested a limited number of mice.

DISCUSSION

Sialylation of oligosaccharide chains is a common and physiologically important event, and sialic acids are probably the

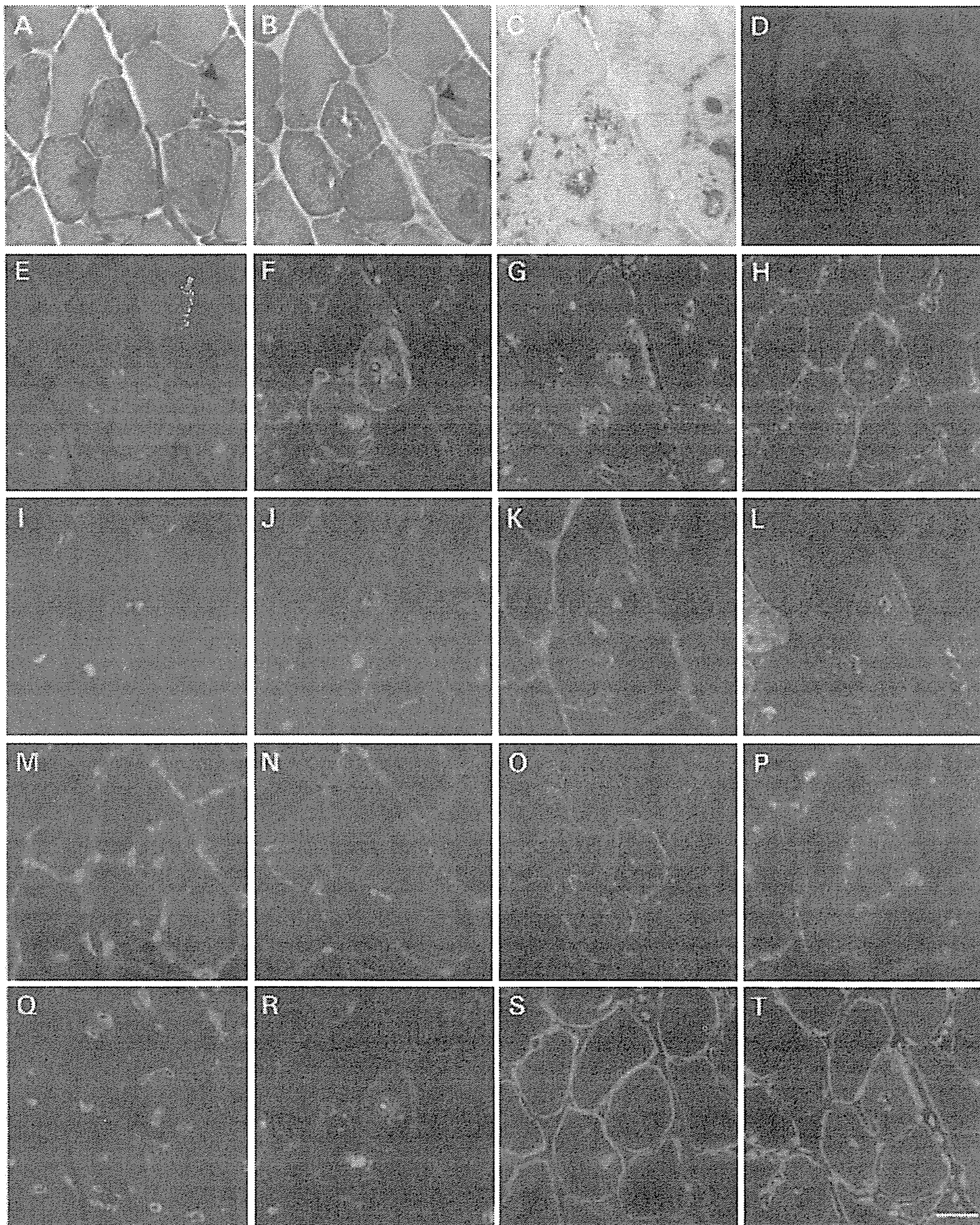

Figure 7. Serial sections taken from a 42-week-old female *Gne*$^{(-/-)}$h*GNE*V572L-Tg mouse. (**A**) Hematoxylin and eosin sections show fibers with RVs and cytoplasmic inclusions. (**B**) In modified Gomori trichrome, vacuoles are rimmed by eosinophilic granules. (**C**) Acid phosphatase activity is enhanced around RVs, suggesting upregulation of lysosomal activity in these areas. (**D**) Congo red staining visualized by Texas red filters shows positive staining in fibers with or without RVs, and appear as large, granular deposits. Immunoreactivity to lysosomal proteins confirm the presence of autophagy in fibers with RVs: (**E**) LAMP-1 signals are seen in the areas of RVs; (**F**) LAMP-2 has subsarcolemmal immunoreactivity, in addition to positive staining in RVs; (**G**) LC3 stains the same areas as LAMP-2, in addition to the perinuclear areas. Intracellular deposition of amyloid is seen in vacuolated or non-vacuolated fibers: (**H**) Increased reactivity to BACE2 is seen in the cytoplasm of fibers with RVs and within the vicinity of RVs; (**I**) AβPP expression is intense in area of RVs, seen as discrete deposits; (**J**) amyloid β 1–42 and (**K**) amyloid β 1–40 stainings are likewise seen as discrete deposits within the vicinity of RVs; (**L**) amyloid β-oligomeric antibody signals are noted as aggregates of small granule-like deposits around the RVs. Neurofilament deposition is observed in the myofibers: SM-31 (**M**) immunoreactivity is occasionally noted within the vicinity of RVs, whereas SM-310 (**N**) only stains intramuscular nerve bundles. (**O**) Epitopes of phosphorylated tau are observed in some fibers with RVs. (**P**) Fibers with RVs have intense ubiquitin staining around RVs and granule-like signals in these fibers. (**Q**) Grp94, an endoplastic reticulum luminal stress protein, is upregulated exclusively in vacuolated fibers as large granular deposits within the RVs. Sarcolemmal proteins are deposited within the vicinity of RVs: (**R**) α-dystroglycan; (**S**) β-dystroglycan; and (**T**) α-sarcoglycan. Bar represents 20 μm.

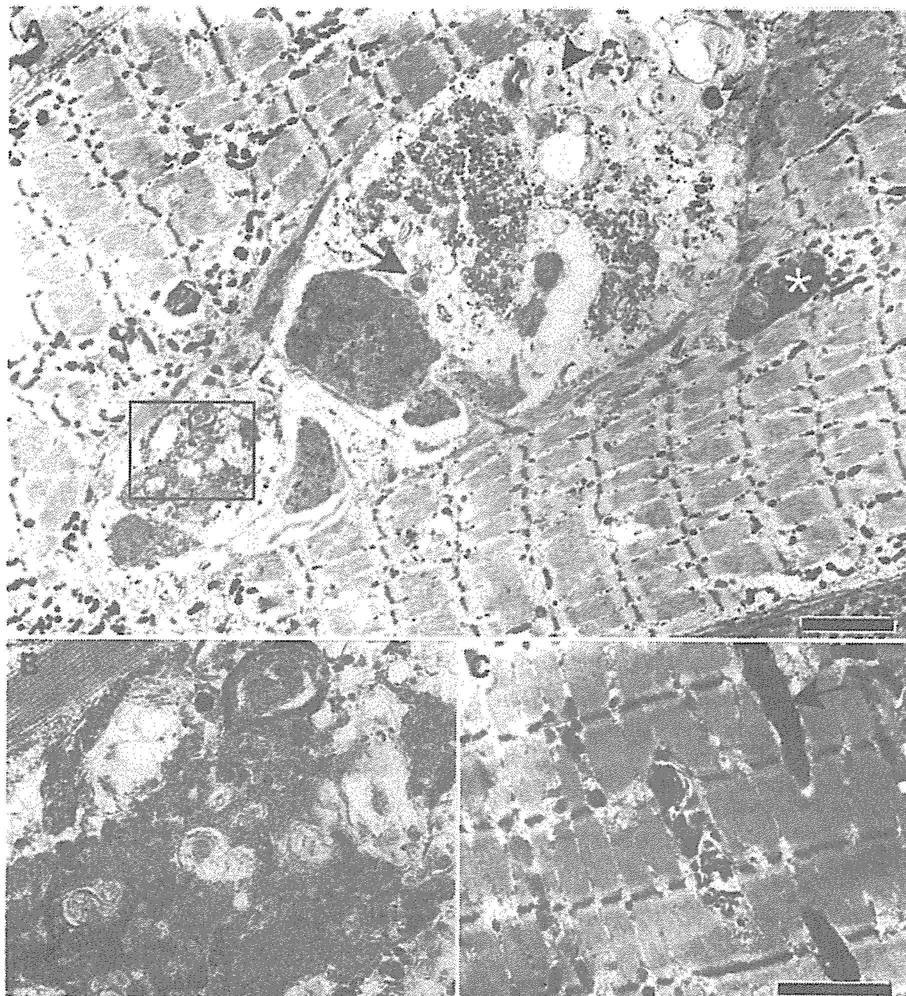

Figure 8. Ultrastructural evidence of autophagy and intracellular inclusions. (A) Collections of lysosomal autophagosomes with intracellular debris which are light or electron-dense amorphous materials enclosed by a limiting membrane (arrow). Multilammelar structures are also observed (double arrows). Ovoid and dense deposits which are probably amyloid deposits are likewise seen (asterisk) (**B**) Probable amyloid deposits are seen as amorphous and granular material surrounded by autophagosomes (B, magnified from A). (**C**) Dense, granular deposits which are probably amyloid accumulations are also noted in areas where architecture of myofibrils are generally well preserved; occasionally, autophagic vacuoles are seen within the substance of these deposits (arrow). Bar represents 2 μm.

most biologically important monosaccharide units of glycoconjugates. These negatively charged sugars at the terminal ends of glycoconjugates have very important biological roles in mammalian development, and this is underscored by the embryonic lethality resulting from attempts to knock-out *Gne* in the mice (20), and further supported by the absence of homozygous null mutations in humans. Making a transgenic *GNE* mouse on a *Gne* knockout background thus allowed us to rescue the phenotype in *Gne* knockout. Clearly, the *Gne*$^{(-/-)}$h*GNE*V572L-Tg resembles the phenotype in human DMRV/h-IBM patients.

It is conceivable that a mutation in the *GNE*, a gene responsible for catalyzing the rate-limiting step in sialic acid biosynthesis, can lead to hyposialylation. Most, if not all, of the mutations causing DMRV caused partial reduction of the enzymatic activity of either UDP-GlcNAc 2-epimerase or ManNAc kinase of the GNE (17,19). As we have predicted, our results show that there is a marked reduction in sialic acid level, which can reflect the enzymatic activity of GNE, in the serum and other tissues of the *Gne*$^{(-/-)}$h*GNE*V572L-Tg mice. With regards to the expression of *GNE* in various tissues, it has been shown that expression in the muscle is very low (25). Our results show, on the other hand, that mRNA expression of h*GNE*V572L-Tg is highest in the muscle, and we attribute this to the promoter that we used in the transgene construct. Previously, we have shown that CAG promoter efficiently promotes expression of a gene into adult skeletal muscles (26).

Skeletal muscle is mainly affected in DMRV/h-IBM, although it is reasonable to expect multi-organ involvement because of the ubiquitous expression of *GNE*. In our mice, the skeletal muscle is clearly affected despite the data that

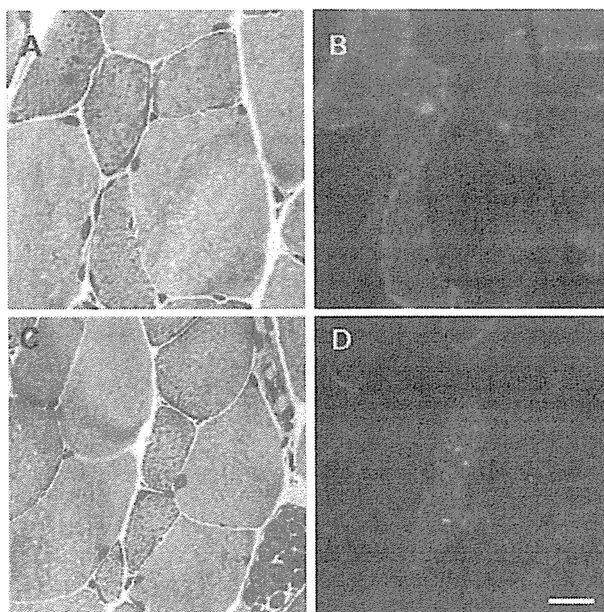

Figure 9. Amyloid deposition precedes RV formation. Sections taken from the gastrocnemius of a 34-week-old female mouse shows variation in fiber size in hematoxylin and eosin sections (A and C). Note the absence of RVs or cytoplamic inclusions in these fibers. Amyloid depositions are seen as immunofluorescent signals in small fibers (**B**, amyloid β 1–42; **D**, AβPP). Bar represents 20 μm.

hyposialylation is not that remarkable when compared with other organs. Our results suggest that even a slight reduction in sialic acid level can cause symptoms in skeletal muscles; however, the selectivity of skeletal muscle may not be explained by the *Gne* expression levels and sialic acid levels in each organ.

It is notable that some of the $Gne^{(-/-)}$h*GNE*V572L-Tg mice die sooner than their littermates, but the precise reason for this is not known at present. It is, however, evident that a significant number of the autopsied mice showed pathological findings in the diaphragm and the heart. In humans, there was a report on two siblings with the homozygous V572L mutation who died from arrhythmia (27), but there had been no reports on respiratory involvement among patients.

The onset of symptoms among DMRV patients has been reported to be from the second to the third decade (3), although there were anecdotal reports of earlier onset (28). Interestingly, in the $Gne^{(-/-)}$h*GNE*V572L-Tg mice, the onset of clinical phenotype is noted around 30 weeks of age, which can be considered to be similar to that in humans, using lifespan and ability to reproduce for points of comparison. It is peculiar that gastrocnemius and quadriceps muscles are preferentially involved in mice, while in humans, the tibialis anterior is remarkably involved while the quadriceps are affected relatively late in the course of the disease. In our recent data on the clinical presentation of DMRV, however, it is clear that the gastrocnemius can be affected more severely in some cases (28).

We tried to check fiber type involvement in these muscles, and found out that both slow and fast fibers are affected in human and mice, in terms of the presence of RVs, but fast type fibers are predominantly involved (data not shown). Sporadic IBM has some pathological similarities with DMRV; recently, it has been shown that the presence of inclusions on routine histochemistry and the pathogenic accumulation of β-amyloid protein occur in fast twitch muscles, both in a transgenic model of IBM and in IBM patients (29), implying that fast type fibers are more vulnerable to pathological changes. Further analysis is needed on this aspect to derive a more conclusive data.

CK levels are reported to be mildly or moderately elevated in patients, although there were isolated cases where the CK activity was above 1000 IU/L (11). CK elevation has always been correlated with the presence of necrotic and regenerating processes in the skeletal muscle, but which are only occasionally found in DMRV/h-IBM. Elevation of serum CK is also seen in the $Gne^{(-/-)}$h*GNE*V572L-Tg mice, although necrotic and regenerating process is barely detectable. Our data suggest that there might be other mechanisms which trigger CK release into the circulation, aside from myonecrosis. It has not been clarified if CK release into the blood stream may be induced by deglycosylation of membrane proteins, although some studies suggested that removal of sialic acids by neuraminidase treatment may influence sarcolemmal permeability (30). Further tests are clearly needed to shed some insight on the CK elevation in DMRV/h-IBM and $Gne^{(-/-)}$ h*GNE*V572L-Tg mice.

A subject of poignant interest is whether RV formation, one of the hallmarks of DMRV/h-IBM, is the primary event that induces muscle fiber atrophy and loss, notwithstanding the fact that RVs are non-specific and could be seen in a multitude of myopathies. In the $Gne^{(-/-)}$h*GNE*V572L-Tg mice, weakness is clearly noted before the occurrence of RVs, implying that other factors should be responsible for the earlier onset of weakness. Consistently, we have documented that serum and other tissues are hyposialylated, and this phenomenon is not at all correlated with age, strongly suggesting that hyposialylation may play a role in the development of clinical manifestations exhibited by patients. Previous studies have implicated that sialic acid directly contributes to the negative surface potential of cells, because desialylation of rat skeletal muscle sodium channel leads to reduced sensitivity of these channels to the effects of external calcium (31). This would mean that voltage gating parameters are shifted to the point that channels required a larger depolarization in order to gate, which may suggest that the mechanism of weakness may be due to the reduced excitability of the muscle membrane as a result of sodium channel desialylation.

The hallmarks of DMRV/h-IBM include RVs that are autophagic in nature (32) and cytoplasmic inclusions in vacuolated and non-vacuolated fibers, both of which are seen in muscle sections from the $Gne^{(-/-)}$h*GNE*V572L-Tg mice. Several proteins have been shown to accumulate in DMRV myofibers (33,34), and most of which have been demonstrated to be mainly associated with amyloid because of the positive reactivity to crystal violet and Congo red, suggesting that they assume the beta-pleated sheet configuration. In general, more than 20 unrelated proteins, including β-amyloid (34), prion, tau (21) and transthyretin, can abnormally unfold and self-aggregate to form beta-pleated sheet amyloid (35). The association of these proteins with DMRV/h-IBM

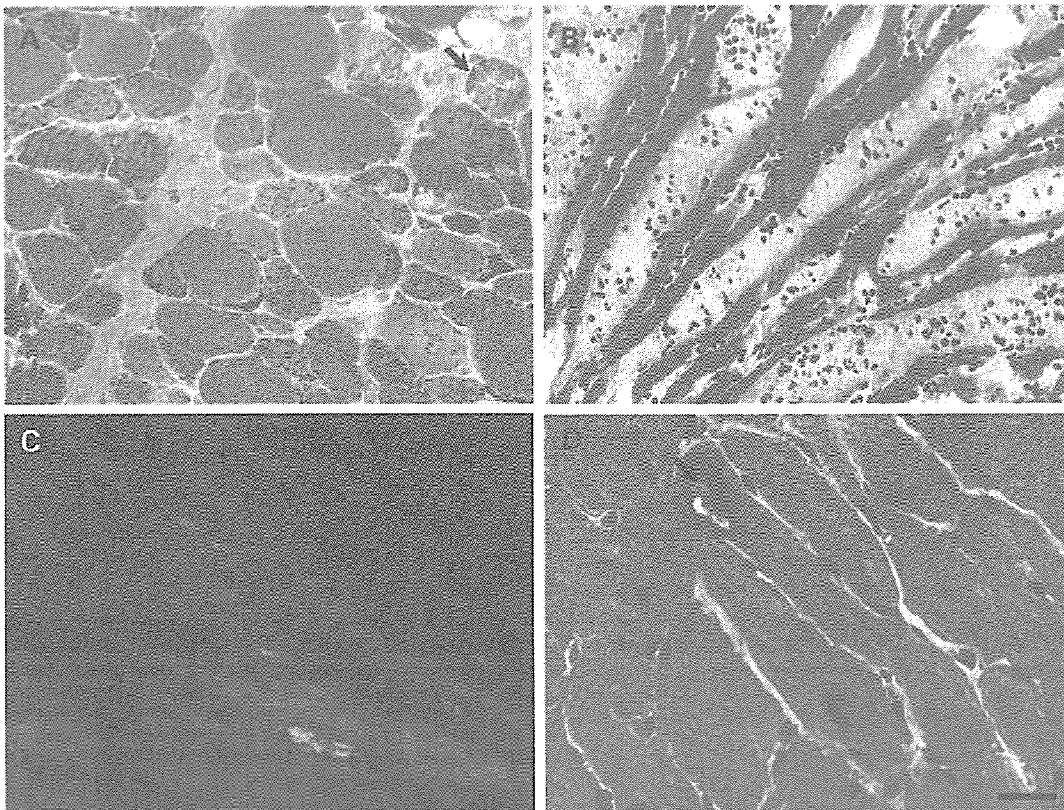

Figure 10. The diaphragm and cardiac muscles are likewise involved in the *Gne*$^{(-/-)}$h*GNE*V572L-Tg mice. (**A**) Modified Gomori trichrome section of a 48-week-old male *Gne*$^{(-/-)}$h*GNE*V572L-Tg. Note the presence of endomysial fibrosis and fiber with RV. (**B**) Hematoxylin and eosin sections from a 54-week-old female *Gne*$^{(-/-)}$h*GNE*V572L-Tg showing marked fibrosis. (**C**) Amyloid deposition (Amyloid β 1–42) is seen in the cardiomyocytes of the same mouse in (B). (**D**) HE section of cardiac muscle from a 42-week-old male *Gne*$^{(-/-)}$h*GNE*V572L-Tg reveals that RVs are occasionally seen in cardiomyocytes.

pathomechanism has largely been enigmatic up to this time, but unfolding and misfolding of proteins most probably play a role. Previous reports have alluded to the role of sialic acid in proper folding of proteins (35–37). The ultimate fate of aggregated, misfolded glycoproteins is degradation, hence the activation of UPR is expected, which could explain the presence of ubiquitin signals in the myofibers of the *Gne*$^{(-/-)}$ h*GNE*V572L-Tg mice and upregulation of ubiquitin and proteasome in DMRV/h-IBM myofibers (38).

The implication of amyloid deposition in the formation of RVs in both DMRV/h-IBM and s-IBM (39) is supported by our finding that the occurrence of amyloid inclusions in the myofibers preceded RV formation. Amyloid itself has been shown *in vitro* to block the degradation of ubiquitinated proteins by inhibiting proteasome activity (40), hence its accumulation may not only lead to cytotoxicity, but also may further aggravate protein misfolding. In addition, it has been clarified that overproduction of amyloid can induce tau hyperphosphorylation and decrease its solubility (41). Sialylation and glycosylation of amyloid precursor protein, which contains both *O*- and *N*-glycans, appear to be important for its proteolytic processing, secretion and metabolism (42–45). Interference with the formation of *N*-linked glycans resulted in a decrease in secreted AβPP and an increase in the level of the cellular form of the protein, which has a higher propensity to form amyloid β peptide (42,46). Although amyloid fibrils were the structure previously considered to be cytotoxic, there is current experimental evidence that pre-amyloid oligomeric complexes or aggregates, either diffuse or in a protofibril stage, can be very cytotoxic (47). The presence of dense deposits in areas with relatively preserved myofibrillar architecture on electron microscopy strongly suggest that deposition of amyloid and amyloid-like structures pre-date RV formation.

Because DMRV/h-IBM patients do not present, in general, with symptoms reflecting involvement of the respiratory system, it is assumed that the diaphragm is relatively spared in this myopathy. In the *Gne*$^{(-/-)}$h*GNE*V572L-Tg mice, it is clear that the diaphragm can be involved, despite the absence of overt respiratory difficulties. The presence of pathological findings in the sacrificed mice, and not only in the ones that died suddenly, may suggest that the presence of RVs *per se*, may not correlate with severity in phenotype, with respect to involvement of diaphragm. A more sensitive method of assessing the respiratory status of these mice, *vis-à-vis* a plain observation, might be helpful in clarifying the extent to which respiratory system is involved. Our results suggest that careful evaluation of respiratory and cardiovascular functions is logical and warranted in human patients.

In the $Gne^{(-/-)}$h*GNE*V572L-Tg mice, we have seen RVs in the cardiac muscles obtained from a couple of mice, clearly supporting the presence of cardiac involvement in DMRV/h-IBM. It has always been reported that DMRV involves primarily skeletal muscles but recently, however, it is being recognized that other organs may likewise be involved. For example, cardiac involvement is not very rare as it is seen in 18% of patients, with a spectrum of manifestations ranging from an incomplete right bundle-branch block to a fatal arrhythmia which led to sudden death (25,26). Sialic acid was shown to be an important component on the surface of heart muscle cells, because its removal reduced the cell surface negative charge by 25% (48) and produced a large increase in cardiac myocyte Ca^{2+}, followed by marked cell contracture (49), emphasizing the importance of negatively charged sialic acid-containing gangliosides in the maintenance of cardiac cell physiological Ca^{2+} permeability. More importantly, it has been demonstrated that in myocardial cells, desialylation of cells by neuraminidase treatment causes aberrant electrical activity (50), and may lead to arrhythmia (51).

In conclusion, we have generated the first mouse model of DMRV/h-IBM, which resembles the clinical, pathological and biochemical features of the disease in humans. The $Gne^{(-/-)}$h*GNE*V572L-Tg mouse is a concrete evidence that mutations in the *GNE* are causative of DMRV/h-IBM. Indeed, these DMRV/h-IBM mice will be a valuable tool to search for further clues in unraveling the pathomechanism of this myopathy. As we have clearly documented in these mice, hyposialylation plays a key role in the pathogenesis of DMRV/h-IBM, and is of paramount importance in considering therapeutic trials.

MATERIALS AND METHODS

Generation of *Gne* knockout mice

The *Gne* knockout mice [$Gne^{(-/-)}$] was produced in inGenious Targeting Laboratory (New York, NY, USA). The 17 kb mouse genomic DNA fragment, containing exons 3–5, was cloned from the mouse 129Sv/Ev lambda genomic library. The Neo cassette that was inserted replaced the 1.4 kb upstream of exon 3, exon 3 and 124 bp downstream of exon 3 (Fig. 1). The resulting targeting vector was linearized by *Not*I, purified and then transfected by electroporation into ES cells. Positive clones after neomycin selection were identified using PCR (primer sequences available upon request).

Generation of h*GNE*V572L-Tg

The cDNA for *GNE* mutant was obtained by reverse transcribed-PCR from skeletal muscle RNA of a DMRV patient with the V572L mutation and cloned into pCR-Blunt vector (Invitrogen, Carlsbad, CA, USA), as described previously (17). Cloned cDNA was sequenced by ABI cycle-sequencing procedures using an ABI 3100 (Applied Biosystems, Foster City, CA, USA). The *Xho*I fragment containing *GNE* mutant cDNA was excised and inserted into pCAGGS vector in which gene expression is driven by a CAG promoter (52). *loxP* sequences were introduced to flank the cDNA insert. *Sal*I fragment was purified and injected into C57BL/6 oocytes and subsequently transplanted into recipient mice. Founders were bred to WT C57BL/6 females to check for germline transmission, which was confirmed by PCR analyses on genomic DNA.

Production of $Gne^{(-/-)}$h*GNE*V572L-Tg

To maintain the same copy number of transgene, stringent measures were taken in generating mice. The h*GNE*V572L-Tg mouse was crossbred to *Gne* heterozygous mouse [$Gne^{(+/-)}$] to create a $Gne^{(+/-)}$ mouse that carried the human *GNE* [$Gne^{(+/-)}$h*GNE*V572L-Tg]. The latter was then mated with a $Gne^{(+/-)}$ mouse, to obtain a mouse that harbors the human V572L mutated *GNE* in a *Gne* knockout background.

For genotyping, DNA was isolated from mouse tails. *Gne* mice genotyping was carried out using PCR analysis on tail genomic DNA with the following primers: Neo, WT3 and S2 (primer sequences available upon request). Further, DNA was digested with *Bam*HI, subjected to Southern blotting and then analyzed by hybridization to a 500 bp probe.

For transgenic mice, the following oligonucleotides were used to amplify a 318 bp segment found specifically in human *GNE*: 1186F, CTTCAAGAGCCACTGCAAA; 1504R, CAATTCCTTCCCGAGGATT.

mRNA expression and determination of copy number

Mouse skeletal muscles, heart, brain, spleen and liver were dissected and rapidly frozen in liquid-nitrogen. Total RNA was extracted from cryostat sections of tissues with TRIzol (Invitrogen) following the manufacturer's protocol. First-strand cDNA was synthesized from RNA by reverse transcription using the Superscript RNase H^- Reverse Transcriptase (Invitrogen) and random hexamers. Gene expression was measured by quantitative real-time PCR in i-Cycler IQ system (Bio-Rad Laboratories, Hercules, CA, USA). Primers (1186F and 1504R) were used to span exon–intron junctions to prevent amplification of genomic DNA. Relative quantification of gene expression was determined by comparison of threshold values as suggested by the manufacturer. All results were normalized with respect to Gapdh expression.

Transgene copy number was determined by the i-Cycler IQ system using the SYBR Green reagent kit according to the manufacturer's instructions. Triplicate samples of tail DNA from transgenic mice of each line were analyzed concurrently against a standard curve of scaled concentrations of an external standard. Primers were designed to amplify the transgene h*GNE*V572L and endogenous *Gne*; twice the ratio of the h*GNE*V572L/*Gne* amplicons was interpreted as copy number.

Sialic acid measurement

The bound sialic acids from the serum and pieces of different tissues were released using 20 mM sulfuric acid hydrolysis for 1 h at 80°C. Free sialic acids were then derivitized with 1, 2-diamino-4, 5-methylenedioxybenzene and analyzed by reverse-phase HPLC fluorescence detection as described previously (53). The eluant was monitored by fluorescence and

Table 1. Antibodies used in the study

Antibody	Manufacturer	Type	Dilution
AβPP (6E10)	Chemicon International Inc., Temecula, CA, USA	Mouse monoclonal	1:1000
Aβ 1–40	Chemicon	Rabbit polyclonal	1:100
Aβ 1–42	Chemicon	Rabbit polyclonal	1:100
Aβ oligomer (A11)	Chemicon	Rabbit polyclonal	1:1000
Human beta site APP cleaving enzyme	Alpha Diagnostic International	Rabbit polyclonal	1:100
Caveolin 3	Transduction Laboratories, Lexington, KY, USA	Rabbit polyclonal	1:400
α-dystroglycan (VIA4-1)	Upstate Cell Signaling Solutions, Lake Placid, NY, USA	Mouse monoclonal	1:100
β-dystroglycan	A gift from Dr Ejiro Ozawa	Rabbit polyclonal	1:200
Grp94 (9G10)	Stressgen Biotechnologies, Calgary, Canada	Rat monoclonal	1:30
LAMP-1 (25)	BD Transduction Laboratories, Lexington, KY, USA	Mouse monoclonal	1:100
LAMP-2A	A gift from Dr Fumitaka Oyama	Rabbit polyclonal	1:100
LC3	A gift from Dr Tamotsu Yoshimori	Rabbit polyclonal	1:200
NCAM (123C3)	Santa Cruz Biotechnology Inc.	Mouse monoclonal	1:100
α-sarcoglycan (Ad1/20A6)	Novocastra Laboratories Ltd.	Mouse monoclonal	1:100
β-sarcoglycan (βSarc/5B1)	Novocastra Laboratories Ltd.	Mouse monoclonal	1:100
polyUbiquitin (FK1)	Biomol International	Mouse monoclonal	1:500
Neurofilament (SM-31)	Sternberg Monoclonals Inc., MD, USA	Mouse monoclonal	1:1000
Neurofilament (SM-310)	Sternberg Monoclonals Inc., MD, USA	Mouse monoclonal	1:1000
tau C	A gift from Dr Fumitaka Oyama	Rabbit polyclonal	1:1000

measured by comparison with Neu5Ac and Neu5Gc standards (from 0.05 nmol/μl to 5 nmol/μl). Total protein from tissues was measured using the Bio-Rad Protein Assay (Bio-Rad Laboratories) according to the manufacturer's protocol.

General assessment for motor strength and fatigability

Whole-animal strength and fatigability were measured according to a test procedure (here referred to as rod-climbing test) previously reported (54). In brief, this test required the mice to pull themselves on top of a suspended rod (3 mM in diameter). The measurement of muscle weakness was based on the mean percentage of passes over 15 trials of the test in a 3-min period. Fatigability was assessed as the average pass rate over time for each group of mice. The test was repeated at least three times after a 2-week period.

Histopathological and histochemical analyses

Fresh specimens from individual skeletal and cardiac muscles were snap-frozen in liquid-nitrogen-cooled isopentane and stored at −80°C until further processing. We stained frozen sections (6 μm) of transversal skeletal and cardiac muscles with a battery of histochemical stains including hematoxylin and eosin, modified Gomori trichrome and acid phosphatase. Sections were analyzed by light microscopy. We performed Congo red staining in 10 μm cryosections following the Putchler's modification, and viewed sections under light microscope and conventional fluorescence microscope using Texas-red filters (39). For immunohistochemical analysis, tissue sections were fixed either in acetone or paraformaldehyde, depending on the primary antibody used, and blocked with 5% normal serum and 2% bovine serum albumin in phosphate-buffered saline. The primary antibodies used are listed in Table 1. We used several antibodies which recognize amyloidβ. 6E10, which is a human-specific antibody, but also reacts to murine tissue when the amyloid burden is high, primarily recognizes AβPP (residues 1–16) after α-secretase cleavage. It also recognizes, in addition, C99 fragment and amyloid β peptides (1–40 and 1–42) which have been shown to be prone to aggregation. The anti-oligomeric antibody (A11) is specific to the oligomeric structure of β amyloid peptides. The following secondary antibodies were used appropriately: anti-goat IgG F (ab′)-2-fragment, FITC conjugated (EY Laboratories, San Mateo, CA, USA); anti-rabbit IgG (H + L), Alexa Fluor conjugated (Molecular Probes, Eugene, OR, USA); anti-mouse IgG1, FITC conjugated (Sanbio/Monosan, Uden, The Netherlands). Images were collected and analyzed with a laser scanning microscope (Olympus, Tokyo, Japan) with its appropriate software.

Morphometric analysis of fibers

Muscle cross sections were stained with rabbit polyclonal antibody against caveolin-3 followed by a fluorescent secondary antibody. Digital images from fluorescence signals were observed under a confocal microscope and the widest diameter was recorded for 600 or more fibers using Image-J software from the public domain NIH Image program (developed at the U.S. National Institutes of Health and available on the Internet at http://rsb.info.nih.gov/nih-image/). Results were analyzed using Statistics Software for Social Sciences (SPSS for Windows, Rel. 11.0.0. 2001, SPSS Inc., Chicago) software.

Electron microscopy

The muscle specimens were immediately fixed for 2 h in 2.5% cold glutaraldehyde with 0.1 M cacodylate buffer, pH 7.3. After washing in cacodylate buffer, the specimens were post-fixed in 1% osmium tetroxide in the same buffer, dehydrated with graded series of ethanol and embedded in Epon. Semi-thin sections (0.5 μm) were stained with toluidine blue alkaline. Ultrathin sections were stained with uranyl acetate, citrated and observed with a H-600 electron microscope (Hitachi, Tokyo, Japan) at 75 kV.

Serum CK

Blood samples were obtained either by inferior vena cava aspiration, or careful collection from mouse tail. Total CK activity was measured by a spectrophotometric assay employing a commercial kit (CPK-L Determiner, Kyowa MEDEX, Tokyo, Japan). For confirmation, CK isoforms were electrophoretically analyzed using Titan Gel CK Isozyme kit (Helena Laboratories, Beaumont, TX, USA) following the manufacturer's protocol.

Statistical analysis

Data were entered in SPSS version 11.0 and were analyzed by computation of the frequency and the mean $\pm$ SD and/or percentage. The data were then subjected to a univariate analysis (Fisher's exact test), Student's *t*-test, Wilcoxon paired test, ANOVA or Mann–Whitney *U* test, log-rank test or multiple regression analysis, whichever was appropriate. *P*-values less than 0.05 were considered to be statistically significant.

ACKNOWLEDGEMENTS

The authors thank the following persons for their invaluable support and assistance: Yoko Keira, Genri Kawahara, Mari Okada and Kumiko Murayama. This study is supported by the 'Research on Psychiatric and Neurological Diseases and Mental Health' from Health and Labour Sciences Research Grants; the 'Research on Health Sciences focusing on Drug Innovation' from the Japanese Health Sciences Foundation; the 'Research Grant (16B-2, 17A-10) for Nervous and Mental Disorders' from the Ministry of Health, Labour and Welfare; and the Program for Promotion of Fundamental Studies in Health Sciences of the National Institute of Biomedical Innovation (NIBIO).

Conflict of Interest statement. None declared.

REFERENCES

1. Nonaka, I., Sunohara, N., Ishiura, S. and Satoyoshi, E. (1981) Familial distal myopathy with rimmed vacuole and lamellar (myeloid) body formation. *J. Neurol. Sci.*, **51**, 141–155.
2. Argov, Z. and Yarom, R. (1984) 'Rimmed vacuole myopathy' sparing the quadriceps. A unique disorder in Iranian Jews. *J. Neurol. Sci.*, **64**, 33–43.
3. Nonaka, I., Noguchi, S. and Nishino, I. (2005) Distal myopathy with rimmed vacuoles and hereditary inclusion body myopathy. *Curr. Neurol. Neurosci. Rep.*, **5**, 61–65.
4. Ikeuchi, T., Asaka, T., Saito, M., Tanaka, H., Higuchi, S., Tanaka, K., Saida, K., Uyama, E., Mizusawa, H., Fukuhara, N. *et al.* (1997) Gene locus for autosomal recessive distal myopathy with rimmed vacuoles maps to chromosome 9. *Ann. Neurol.*, **41**, 432–437.
5. Mitrani-Rosenbaum, S., Argov, Z., Blumenfeld, A., Seidman, C.E. and Seidman, J.G. (1996) Hereditary inclusion body myopathy maps to chromosome 9p1-q1. *Hum. Mol. Genet.*, **5**, 159–163.
6. Nishino, I., Noguchi, S., Murayama, K., Driss, A., Sugie, K., Oya, Y., Nagata, T., Chida, K., Takahashi, T., Takusa, Y. *et al.* (2002) Distal myopathy with rimmed vacuoles is allelic to hereditary inclusion body myopathy. *Neurology*, **59**, 1689–1693.
7. Eisenberg, I., Avidan, N., Potikha, T., Hochner, H., Chen, M., Olender, T., Barash, M., Shemesh, M., Sadeh, M., Grabov-Nardini, G. *et al.* (2001) The UDP-*N*-acetylglucosamine 2-epimerase/*N*-acetylmannosamine kinase gene is mutated in recessive hereditary inclusion body myopathy. *Nat. Genet.*, **29**, 83–87.
8. Keppler, T., Hinderlich, S., Langner, J., Scwartz-Albiez, R., Reutter, W. and Pawlita, M. (1999) UDP-GlcNAc 2-epimerase: a regulator of cell surface sialylation. *Science*, **284**, 1372–1376.
9. Eisenberg, I., Grabov-Nardini, G., Hochner, H., Korner, M., Sadeh, M., Bertorini, T., Bushby, K., Castellan, C., Felice, K., Mendell, J. *et al.* (2003) Mutations spectrum of *GNE* in hereditary inclusion body myopathy sparing the quadriceps. *Hum. Mutat.*, **21**, 99.
10. Argov, Z., Eisenberg, I., Grabov-Nardini, G., Sadeh, M., Wirguin, I., Soffer, D. and Mitrani-Rosenbaum, S. (2003) Hereditary inclusion body myopathy: the Middle Eastern genetic cluster. *Neurology*, **60**, 1519–1523.
11. Tomimitsu, H., Shimizu, J., Ishikawa, K., Ohkoshi, N., Kanazawa, I. and Mizusawa, H. (2004) Distal myopathy with rimmed vacuoles (DMRV): new *GNE* mutations and splice variant. *Neurology*, **62**, 1607–1610.
12. Kim, B.J., Ki, C.S., Kim, J.W., Sung, D.H., Choi, Y.C. and Kim, S.H. (2006) Mutation analysis of the *GNE* gene in Korean patients with distal myopathy with rimmed vacuoles. *J. Hum. Genet.*, **51**, 137–140.
13. Ro, L.S., Lee-Chen, G.J., Wu, Y.R., Lee, M., Hsu, P.Y. and Chen, C.M. (2005) Phenotypic variability in a Chinese family with rimmed vacuolar distal myopathy. *J. Neurol. Neurosurg. Psychiatry*, **76**, 752–755.
14. Broccolini, A., Ricci, E., Cassandrini, D., Gliubizzi, C., Bruno, C., Tonoli, E., Silvestri, G., Pescatori, M., Rodolico, C., Sinicropi, S. *et al.* (2004) Novel *GNE* mutations in Italian families with autosomal recessive hereditary inclusion-body myopathy. *Hum. Mutat.*, **23**, 632.
15. Liewluck, T., Pho-Iam, T., Limwongse, C., Thongnoppakhun, W., Boonyapisit, K., Raksadawan, N., Murayama, K., Hayashi, Y.K., Nishino, I. and Sangruchi, T. (2006) Mutation analysis of the *GNE* gene in distal myopathy with rimmed vacuoles (DMRV) patients in Thailand. *Muscle Nerve*, Epub ahead of print.
16. Amouri, R., Driss, A., Murayama, K., Kefi, M., Nishino, I. and Hentati, F. (2005) Allelic heterogeneity of *GNE* gene mutation in two Tunisian families with autosomal recessive inclusion body myopathy. *Neuromuscul. Disord.*, **15**, 361–363.
17. Noguchi, S., Keira, Y., Murayama, K., Ogawa, M., Fujita, M., Kawahara, G., Oya, Y., Imazawa, M., Goto, Y., Hayashi, *et al.* (2004) Reduction of UDP-*N*-acetylglucosamine 2-epimerase/*N*-acetylmannosamine kinase activity and sialylation in distal myopathy with rimmed vacuoles. *J. Biol. Chem.*, **279**, 11402–11407.
18. Salama, I., Hinderlich, S., Shlomai, Z., Eisenberg, I., Krause, S., Yarema, K., Argov, Z., Lochmuller, H., Reutter, W., Dabby, R. *et al.* (2005) No overall hyposialylation in hereditary inclusion body myopathy myoblasts carrying the homozygous M712T GNE mutation. *Biochem. Biophys. Res. Commun.*, **328**, 221–226.
19. Hinderlich, S., Salama, I., Eisenberg, I., Potikha, T., Mantey, L.R., Yarema, K.J., Horstkorte, R., Argov, Z., Sadeh, M., Reutter, W. *et al.* (2004) The homozygous M712T mutation of UDP-*N*-acetylglucosamine 2-epimerase/*N*-acetylmannosamine kinase results in reduced enzyme activities but not in altered overall cellular sialylation in hereditary inclusion body myopathy. *FEBS Lett.*, **566**, 105–109.
20. Schwarzkopf, M., Knobeloch, K.P., Rohde, E., Hinderlich, S., Wiechens, N., Lucka, L., Horak, I., Reutter, W. and Horstkorte, R. (2002) Sialylation is essential for early development in mice. *Proc. Natl Acad. Sci. USA*, **99**, 5267–5270.
21. Mirabella, M., Alvarez, R.B., Bilak, M., Engel, W.K. and Askanas, V. (1996) Difference in expression of phosphorylated tau epitopes between sporadic and hereditary inclusion-body myopathies. *J. Neuropathol. Exp. Neurol.*, **55**, 774–786.
22. Akanas, V. and Engel, W.K. (2006) Inclusion-body myositis: a myodegenerative conformational disorder associated with Abeta, protein misfolding, and proteasome inhibition. *Neurology*, **66** (Suppl. 1), S39–S48.
23. Askanas, V. and Engel, W.K. (2003) Hereditary inclusion myopathies. In Rosenberg, R.N., Prusiner, S.B., DiMauro, S., Barchi, R.L. and Nestler, E.J. (eds), *The Molecular and Genetic Basis of Neurologic and Psychiatric Disease*, 3rd edn. Butterworth–Heinemann, Woburn, MA, USA, pp. 501–509.
24. Akanas, V. and Engel, W.K. (2003) Proposed pathogenic cascade of inclusion-body myositis: importance of amyloid-beta, misfolded proteins, predisposing genes, and aging. *Curr. Opin. Rheumatol.*, **15**, 734–744.
25. Horstkorte, R., Nöhring, S., Wiechens, N., Schwarzkopf, M., Danker, K., Reutter, W. and Lucka, L. (1999) Tissue expression and amino acid sequence of murine UDP-*N*-acetylglucosamine-2-epimerase/*N*-acetylmannosamine kinase. *FEBS J.*, **260**, 923–927.

26. Ishii, A., Hagiwara, Y., Saito, Y., Yamamoto, K., Yuasa, K., Sato, Y., Arahata, K., Shoji, S., Nonaka, I., Saito, I., Nabeshima, Y., Takeda, S. (1999) Effective adenovirus-mediated gene expression in adult murine skeletal muscle. *Muscle Nerve*, **22**, 592–599.
27. Kimpara, T., Imamura, T., Tsuda, T., Sato, K. and Tsuburaya, K. (1993) Distal myopathy with rimmed vacuoles and sudden death—report of two siblings. *Rinsho Shinkeigaku*, **33**, 886–890.
28. Nishino, I., Malicdan, M.C., Murayama, K., Nonaka, I., Hayashi, Y.K. and Noguchi, S. (2005) Molecular pathomechanism of distal myopathy with rimmed vacuoles. *Acta Myol.*, **24**, 80–83.
29. Sugarman, M., Kitazawa, M., Baker, M., Caiozzo, V.J., Querfurth, H.W. and LaFerla, F.M. (2006) Pathogenic accumulation of APP in fast twitch muscle of IBM patients and a transgenic model. *Neurobiol. Aging*, **27**, 423–432.
30. Post, J.A. (1992) Removal of sarcolemmal sialic acid residues results in a loss of sarcolemmal functioning and integrity. *Am. J. Physiol.*, **263**, H147–H152.
31. Bennett, E., Urcan, M.S., Tinkle, S.S., Kozkowski, A. and Levinson, S. (1997) Contribution of sialic acid to the voltage dependence of sodium channel gating: a possible electrostatic mechanism. *J. Gen. Physiol.*, **109**, 327–343.
32. Nishino, I. (2003) Autophagic vacuolar myopathies. *Curr. Neurol. Neurosci. Rep.*, **3**, 64–69.
33. Askanas, V., Alvarez, R.B. and Engel, W.K. (1993) β-Amyloid precursor epitopes in muscle fibers of inclusion body myositis. *Ann. Neurol.*, **34**, 551–560.
34. Askanas, V. and Engel, W.K. (1995) New advances in the understanding of sporadic inclusion-body myositis and hereditary inclusion-body myopathies. *Curr. Opin. Rheumatol.*, **7**, 486–496.
35. Ellis, R. and Pinheiro, T.J.T. (2002) Danger: misfolding proteins. *Nature*, **416**, 483–484.
36. Brooks, S.A., Dwek, M.V. and Schumacher, U. (2002) *Functional and Molecular Gycobiology*. BIOS Scientific Publishers Limited, Oxford, UK.
37. Helenius, A. and Aebi, M. (2004) Roles of *N*-linked glycans in the endoplasmic reticulum. *Annu. Rev. Biochem.*, **73**, 1019–1049.
38. Kumamoto, T., Fujimoto, S., Nagao, S., Masuda, T., Sugihara, R., Ueyama, H. and Tsuda, T. (1998) Proteasomes in distal myopathy with rimmed vacuoles. *Intern. Med.*, **37**, 746–752.
39. Askanas, V., Engel, W.K. and Alvarez, R.B. (1993) Enhanced detection of congo-red-positive amyloid deposits in muscle fibers of inclusion body myositis and brain of Alzheimer's disease using fluorescence technique. *Neurology*, **43**, 1265–1267.
40. Gregori, L., Hainfeld, J.F., Simon, M.N. and Goldbager, D. (1997) Binding of amyloid β protein to the 20S proteasome. *J. Biol. Chem.*, **272**, 58–62.
41. Wang, Y.P., Wang, X.C., Tian, Q., Yang, Y., Zhang, Q., Zhang, J.Y., Zhang, Y.C., Wang, Z.F., Wang, Q., Li, H. *et al.* (2006) Endogenous overproduction of β-amyloid induces tau hyperphosphorylation and decreases the solubility of tau in N2a cells. *J. Neural. Transm.*, Epub ahead of print.
42. McFarlane, I., Georgopoulou, N., Coughlan, C.M., Gillian, A.M. and Breen, K.C. (1999) The role of the protein glycosylation state in the control of cellular transport of the amyloid beta precursor protein. *Neuroscience*, **90**, 15–25.
43. Pahlsson, P. and Spitalnik, S.L. (1996) The role of glycosylation in synthesis and secretion of beta-amyloid precursor protein by Chinese hamster ovary cells. *Arch. Biochem. Biophys.*, **331**, 177–186.
44. Yazaki, M., Tagawa, K., Maruyama, K., Sorimachi, H., Tsuchiya, T., Ishiura, S. and Suzuki, K. (1996) Mutation of potential *N*-linked glycosylation sites in Alzheimer's disease amyloid precursor protein (APP). *Neurosci. Lett.*, **221**, 57–60.
45. Nakagawa, K., Kitazume, S., Oka, R., Maruyama, K., Saido, T.C., Sato, Y., Endo, T. and Hashimoto, Y. (2006) Sialylation enhances the secretion of neurotoxic amyloid-beta peptides. *J. Neurochem.*, **96**, 924–933.
46. Georgopoulou, N., McLaughlin, M., McFarlane, I. and Breen, K.C. (2001) The role of post-translational modification in beta-amyloid precursor protein processing. *Biochem. Soc. Symp.*, **67**, 23–36.
47. Tsai, B., Ye, Y. and Rapoport, T.A. (2002) Retro-translocation of proteins from the endoplasmic reticulum into the cytosol. *Nat. Rev. Mol. Cell Biol.*, **3**, 246–255.
48. Soeiro, M.N., Silva-Filho, F.C. and Meirelles, M.N. (1994) The nature of anionic sites and the endocytic pathway in heart muscle cells. *J. Submicrosc. Cytol. Pathol.*, **26**, 121–130.
49. Marengo, F.D., Wang, S.Y., Wang, B. and Langer, G.A. (1998) Dependence of cardiac cell Ca^{2+} permeability on sialic acid-containing sarcolemmal gangliosides. *J. Mol. Cell Cardiol.*, **30**, 127–137.
50. Woods, W.T., Inamura, K. and James, T.R. (1982) Electrophysiological and electron microscopic correlations concerning the effects of neuraminidase on canine heart cells. *Circ. Res.*, **50**, 228–231.
51. Ufret-Vincenty, C.A., Baro, D.J. and Santana, L.F. (2001) Differential contribution of sialic acid to the function of repolarizing K^+ currents in ventricular myocytes. *Am. J. Physiol. Cell Physiol.*, **281**, C464–C474.
52. Niwa, H., Yamamura, K. and Miyazaki, J. (1991) Efficient selection for high-expression transfectants with a novel eukaryotic vector. *Gene*, **108**, 193–199.
53. Hara, S., Yamaguchi, M., Takemori, Y., Nakamura, M. and Ohkura, Y. (1986) Highly sensitive determination of *N*-acetyl- and *N*-glycolylneuraminic acids in human serum and urine and rat serum by reversed-phase liquid chromatography with fluorescence detection. *J. Chromatogr.*, **377**, 111–119.
54. Keppler, O.T., Hinderlich, S., Langner, J., Schwartz-Albiez, R., Reutter, W. and Pawlita, M. (1999) UDP-GlcNAc 2-epimerase: a regulator of cell surface sialylation. *Science*, **284**, 1372–1376.

Acta Myologica • 2005; XXIV: p. 80-83

Molecular pathomechanism of distal myopathy with rimmed vacuoles

I. Nishino, May Christine V. Malicdan, K. Murayama, I. Nonaka, Y.K. Hayashi, S. Noguchi

Department of Neuromuscular Research, National Institute of Neuroscience, National Center of Neurology and Psychiatry (NCNP), Kodaira, Tokyo, Japan

Distal myopathy with rimmed vacuoles (DMRV) and hereditary inclusion body myopathy (HIBM) are now known to be the same disease and are caused by mutations in the *GNE* gene that encodes a bifunctional protein with two enzymatic activities: UDP-GlcNAc2-epimerase (GNE) and ManNAc kinase (MNK). GNE catalyzes the rate-limiting step in the sialic acid biosynthesis and MNK catalyzes the next step.

So far, we have found homozygous or compound heterozygous mutations in 55 unrelated Japanese DMRV patients. Among them, c.1714G>C (p.V572L) mutation is the most common, accounting for 57% of the mutant alleles. The same mutation was recently identified also in Korean DMRV patients, raising the possibility of the presence of a common founder. We have also found that cardiac involvement is not very rare and is found in 18% of patients, albeit degree of severity widely varies; in some patients, it can result in sudden death. The length of time when patients become non ambulatory is diverse. The severity of clinical symptoms also varies widely, as evidenced by the presence of an asymptomatic homozygote harboring of p.D176V, the second most common mutation among Japanese patients.

Patients' fibroblasts and myotubes are hyposialylated and this hyposialylation can be recovered by adding GNE metabolite, ManNAc, or sialic acid per se, NeuAc. Accordingly, the sialylation status in the skeletal muscle tissue is also greatly altered especially in fibers with rimmed vacuoles, suggesting the tight association between hyposialylation and the formation of rimmed vacuoles. However, we still do not know why hyposialylation leads to the formation of rimmed vacuoles. To further elucidate the pathomechanism and to develop a therapy of DMRV, we need to produce mouse model mouse for this disease.

Key words: DMRV, HIBM, rimmed vacuole, sialylation

Clinical features

Distal myopathy with rimmed vacuoles (DMRV) is an autosomal recessive muscle disorder affecting young adults and was originally described by Nonaka et al. in 1981, and thus it is also called Nonaka myopathy [1-4]. This disease has been known to be clinicopathologically similar to hereditary inclusion body myopathy (HIBM), which was earlier described as "rimmed vacuole myopathy" sparing the quadriceps by Argov et al. in 1983 [5]. DMRV and HIBM were initially described in Japanese and Iranian Jews, respectively; at present, however, patients with these diseases are seen all over the world. In addition, as I will discuss later, DMRV and HIBM are now known to be the same disease [6].

DMRV/HIBM is characterized clinically by the preferential involvement of tibialis anterior muscle sparing the quadriceps muscles [1-5]. The age at onset ranges from 15 to 40 years with an average of 26 years. The initial symptom is usually altered gait. Patients become wheelchair-bound between 26 and 57 years of age, on average 12 years after the onset of symptoms. Muscle biopsy is characterized by the presence of many rimmed vacuoles especially in atrophic fibers. Necrotic and regenerating fibers are rarely seen. The rimmed vacuoles occasionally contain congophilic amyloid material and deposits that are immunoreactive to β-amyoid and β-amyloid precursor protein, ubiquitin and tau protein. The nucleus occasionally contains tubulofilamentous inclusions of 15-20 nm in diameter [2-4].

Genetic cause

Both DMRV and HIBM had been mapped to chromosome 9 by two independent linkage analyses [7, 8]. In 2001, Israeli group identified that HIBM is associated with mutations in the *GNE* gene which encodes a bifunctional enzyme, UDP-N-acetylglucosamine 2-

Address for correspondence: Ichizo Nishino, M.D., Ph.D., Department of Neuromuscular Research, National Institute of Neuroscience, National Center of Neurology and Psychiatry (NCNP), 4-1-1 Ogawahigashi-cho, Kodaira, Tokyo 187-8502, Japan, Tel: +81-42-341-2711 ext 5111, Fax: +81-42-346-1742, E-mail: nishino@ncnp.go.jp

epimerase (GNE)/N-acetylmannosamine kinase (MNK) [9]. Most of the mutations were missense, including the most common p.M712T among Iranian Jews, and only a few null mutations were found. In addition, no patient had null mutations in both alleles. This result well fits the fact that knocking out the *GNE* gene causes early embryonic lethality in mice [10].

The identification of the causative gene for HIBM led us to evaluate our DMRV patients for GNE mutations. We initially screened 27 unrelated patients with DMRV for mutations in the GNE gene [6] and later additionally analyzed 27 patients. Our results were similar to those of Israeli group. All mutations were missense except for one exon skipping mutation. The c.1714G>C (p.V572L) mutation was the most commonly encountered, followed by the c.527A>T (p.D176V) mutation, accounting for 57% and 24% of alleles, respectively. The p.V572L mutation was recently identified also in Korean DMRV patients, raising a possibility of the presence of a common founder (Personal communication with Dr. Chang-Seok Ki, Samsung Medical Center, Seoul, Korea).

The identification of the causative gene now allows us to better demarcate the clinical spectrum of DMRV/HIBM, which, in fact, has turned out to be more heterogenous than previously thought. First, DMRV/HIBM had been considered to involve only skeletal muscle; however, we found that cardiac involvement is not very rare as it is , seen in 18% of patients, albeit severity widely varies from an incomplete right bundle-branch block to sudden death due to arrhythmia which led to sudden death. This indicates that even in patients with no apparent cardiac abnormality, careful examination of the cardiac function is necessary. Second, the duration of time when patients become non-ambulatory is more variable than previously considered, ranging from 3 to 22 years, based upon data from Niigata University (Dr. Keiko Tanaka, Personal communication). Third, the disease usually starts from muscle weakness in the lower extremities; there are patients, however, in some exceptional cases who show severe hand muscle weakness even while they are still ambulant. Fourth, tibialis anterior muscle is preferentially affected in most cases; but gastrocnemius muscle is more severely affected in rare cases. Lastly, the spectrum of disease severity is immensely diversified. The ultimate example may be an individual with a homozygous p.D176V, the second most common mutation among Japanese patients, who remains to be asymptomatic to date. He was serendipitously identified during a screening of the mutations in the family members of a DMRV patient. Now at the age of 64 years, he still is able to work as a Tatami (traditional Japanese mat) craftsman and carries heavy Tatami by himself. He has no muscle weakness or atrophy, including tibialis anterior and hamstrings. The presence of such an asymptomatic homozygote suggests that presence of *GNE* mutations may not be the only determining factor and that there may be a mitigating factor [6] still to be discovered.

Enzymatic activity

The identification of mutations in the GNE gene naturally raised a question of whether enzymatic activity is decreased in patients. To address this question, we first measured the epimerase activity in patients' leukocytes using tritium-labeled UDP-GlcNAc [6]. It was markedly decreased in terms of the mean value. However, the error bar was too big to use this enzymatic assay as a diagnostic test for each case. To more precisely determine the enzymatic activity and also to separately distinguish the activities of epimerase and kinase, we produced recombinant proteins with the mutations that we identified. As expected, all missense mutants showed decreased enzymatic activities [11]. In addition, most mutations respectively affected the corresponding enzymatic activities, i.e., mutation in the epimerase domain resulted in decreased GNE activity while the mutation is in the kinase domain. Our results indicate that DMRV/HIBM is caused by the loss-of-function in the *GNE* gene.

Hyposialylation

Since GNE catalyzes the rate-limiting step in the sialic acid biosynthesis while MNK catalyzes the next step, and because GNE and/or MNK enzymatic activities, are decreased in recombinant proteins, it is reasonable to hypothesize that sialic acid level may be decreased in patients' cells and tissues. We therefore evaluated the sialylation status in patients' fibroblasts and myotubes using several lectins [11]. Lectins are proteins often of plants that recognize and bind to specific sugar chain structures on glycoproteins and/or glycolipids. The panel of lectins that we used includes wheat germ agglutinin (WGA) and soybean agglutinin (SBA) that detect clustered sialic acid and Galα1->3GalNac structures, respectively. In patients' fibroblasts, signals detected by WGA were decreased while those by SBA were increased, suggesting that the cells were hyposialylated and GalNAc is alterna-

tively exposed in the cell surface. To confirm that this hyposialylation is due to the *GNE* gene defect, we evaluated the sialylation status after adding the substrate and metabolite of GNE, GlcNac and ManNAc, respectively. As expected, the hyposialylated status was not affected by GlcNAc while it was recovered by ManNAc, clearly demonstrating that this hyposialylation is due to GNE defect. The same phenomenon was also observed with the addition of the final product of the sialic acid biosynthesis pathway, NeuAc or NANA. Furthermore, we also performed the same experiment using patients' myotubes. When we deprived serum from the culture media, WGA's signal was decreased while SBA's was increased, a finding similar to that in fibroblasts. When we added ManNAc or NeuAc but not GlcNAc, this hyposialylation was recovered. Quantitative analysis showed that sialic acid level was reduced to 60-75% of control. Furthermore, sialylation abnormality was also confirmed in muscle tissue, again using lectins. Overall, our results raise the possibility of developing a therapy using these compounds.

Interestingly, the serum sialic acid level in DMRV/HIBM patients was normal, indicating that even with the loss-of-function-type missense mutations, patients have a minimal enzymatic activity enough to maintain the sialic acid level in the serum [11]. This is probably because GNE expression in other organs, such as liver and saliva, is very high and even if it is reduced, remaining enzymatic activity can compensate for the loss. In the skeletal muscle, in contrast, GNE expression is quite low. Most likely, in skeletal muscle, sialic acid level is maintained by what little GNE it has so it may not be able to compensate for the loss of enzymatic activity due to *GNE* mutation.

Pathomechanism

In muscles from DMRV/HIBM patients, a variety of abnormalities are seen including amyloid deposition [12], abnormal phosphorylation of tau [13], tubulofilamentous inclusion [2-4], rimmed vacuoles [2-4], activation of ubiquitin proteasome sys-

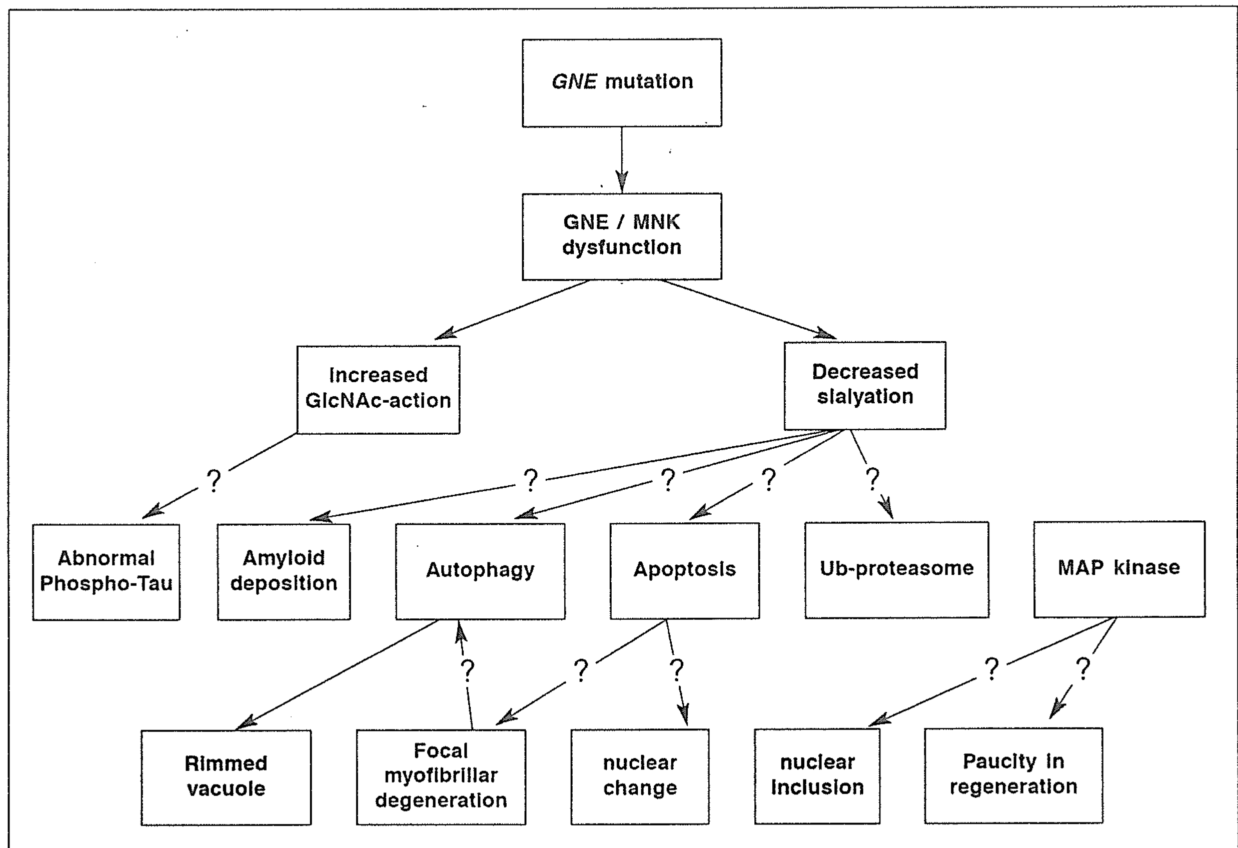

Figure 1. Schematic illustration of the pathomechanism of DMRV/HIBM. There are a variety of abnormalities in skeletal muscle in DMRV/HIBM; however, it is still unknown how the hyposialylation leads to such abnormalities.

tem [14], and apoptosis [15]. Now, we know that the loss-of-function mutations in the *GNE* gene cause the hyposialylation of skeletal muscle; nevertheless, there still remains a mystery of how this hyposialylation leads to a variety of abnormalities (Fig. 1). To answer this question and to develop a therapy for DMRV/HIBM, we need to produce an animal model with a missense mutation in the GNE gene since a null mutation is embryonically lethal [10].

Acknowledgments

We thank Drs. Masashi Aoki, Tohoku University, Sendai Japan; Keiko Tanaka, Niigata University, Niigata, Japan; and Chang-Seok Ki, Samsung Medical Center, Seoul, Korea; for sharing unpublished data. This study is supported partly by the "Research on Health Sciences focusing on Drug Innovation" and the "Research on Psychiatric and Neurological Diseases and Mental Health" from the Japanese Health Sciences Foundation; partly by the "Grant-in-Aid for Scientific Research" from the Japan Society for the Promotion of Science; partly by the "Research on Psychiatric and Neurological Diseases and Mental Health" from Health and Labour Sciences Research Grants; partly by the Program for Promotion of Fundamental Studies in Health Sciences of the National Institute of Biomedical Innovation (NIBIO); and partly by the "Research Grant (17A-10) for Nervous and Mental Disorders" from the Ministry of Health Labour and Welfare.

References

1. Nonaka I, Sunohara N, Ishiura S, Satoyoshi E. Familad distal myopathy with rimmed vacuole and lamellar (myeloid) body formation. J Neurol Sci 1981;51:141-55.
2. Nonaka I, Murakami N, Suzuki Y, Kawai M. Distal myopathy with rimmed vacuoles. Neuromuscul Disord 1998;8:333-7.
3. Nonaka I. Distal myopathies. Curr Opin Neurol 1999;12:493-9.
4. Nonaka I, Murakami N, Suzuki Y, Kawai M. Distal myopathy with rimmed vacuoles. Neuromuscul Disord 1988;8:333-7.
5. Argov Z, Yarom R. 'Rimmed vacuole myopathy' sparing the quadriceps. A unique disorder in Iranian Jews. J Neurol Sci 1984;64: 33-43.
6. Nishino I, Noguchi S, Murayama K, et al. Distal myopathy with rimmed vacuoles is allelic to hereditary inclusion body myopathy. Neurology 2002;59:1689-93.
7. Mitrani-Rosenbaum S, Argov Z, Blumenfeld A, et al. Herediatry inclusion body myopathy maps to chromosome 9p1-q1. Hum Mol Genet 1996;5:159-63.
8. Ikeuchi T, Asaka T, Saito M, et al. Gene locus for autosomal recessive distal myopathy with rimmed vacuoles maps to chromosome 9. Ann Neurol 1997;41:432-7.
9. Eisenberg I, Avidan N, Potikha T, et al. The UDP-N-acetylglucosamine 2-epimerase/N-acetylmannosamine kinase gene is mutated in recessive hereditary inclusion body myopathy. Nat Genet 2001;29:83-7.
10. Schwarzkopf M, Knobelch KP, Orhde E, et al. Sialylation is essential for early development in mice. Proc Natl Acad Sci USA 2002;99:5267-70.
11. Noguchi S, Keira Y, Murayama K, et al. Reduction of UDPN acetylglucosamine 2-epimerase/N-acetylmannosamine kinase activity and sialylation in distal myopathy with rimmed vacuoles. J Biol Chem 2004;279:11402-7.
12. Askanas V, Engel WK. New advances in the understanding of sporadic inclusion-body myositis and hereditary inclusion body myopathies. Curr Opin Rheumatol 1995;7:486-96.
13. Mirabella M, Alvarez RB, Bilak M, et al. Difference in expression of phosphorylated tau epitopes between sporadic and hereditary inclusion-body myopathies. J Neuropathol Exp Neurol 1996;55:774-86.
14. Kumamoto T, Fujimoto S, Nagao S, et al. Proteasomes in distal myopathy with rimmed vacuoles. Intern Med 1998;37:746-52.
15. Yan C, Ikezoe K, Nonaka I. Apoptotic muscle fiber degeneration in distal myopathy with rimmed vacuoles. Acta Neuropathol 2001;101:9-16.

NEUROLOGY

A new congenital form of X-linked autophagic vacuolar myopathy
C. Yan, M. Tanaka, K. Sugie, T. Nobutoki, M. Woo, N. Murase, Y. Higuchi, S. Noguchi, I. Nonaka, Y. K. Hayashi and I. Nishino
Neurology 2005;65;1132-1134
DOI: 10.1212/01.wnl.0000178979.19887.f5

This information is current as of February 6, 2006

The online version of this article, along with updated information and services, is located on the World Wide Web at:
http://www.neurology.org/cgi/content/full/65/7/1132

Neurology is the official journal of AAN Enterprises, Inc. A bi-monthly publication, it has been published continuously since 1951. Copyright © 2005 by AAN Enterprises, Inc. All rights reserved. Print ISSN: 0028-3878. Online ISSN: 1526-632X.

Downloaded from www.neurology.org by LISA TIANO on February 6, 2006

A new congenital form of X-linked autophagic vacuolar myopathy

Abstract—In a new family with X-linked congenital autophagic vacuolar myopathy (AVM), seven affected boys presented with congenital hypotonia, dyspnea, and dysphagia with delayed motor milestones. Muscle pathology revealed autophagic vacuoles with sarcolemmal features, multilayered basal lamina with marked sarcolemmal deposition of C5-9 membrane attack complex and calcium, histologically indistinguishable from childhood-onset X-linked myopathy with excessive autophagy (XMEA). Haplotype analysis suggests that this new AVM and XMEA may be allelic despite different clinical presentations.

NEUROLOGY 2005;65:1132–1134

C. Yan, MD; M. Tanaka, PhD; K. Sugie, MD, PhD; T. Nobutoki, MD; M. Woo, MD; N. Murase, MD, PhD; Y. Higuchi, MD, PhD; S. Noguchi, PhD; I. Nonaka, MD, PhD; Y.K. Hayashi, MD, PhD; and I. Nishino, MD, PhD

Autophagic vacuolar myopathy (AVM) is pathologically characterized by presence of autophagic vacuoles with sarcolemmal features (AVSF)—autophagic vacuoles with expression of virtually all sarcolemmal proteins and acetylcholinesterase (AChE).[1] Four forms of AVM with AVSF have been identified: Danon disease,[2] X-linked myopathy with excessive autophagy (XMEA),[3] infantile AVM,[4] and adult-onset AVM with multiorgan involvement.[5] Danon disease is an X-linked dominant disorder with LAMP-2 gene (LAMP-2) mutation on chromosome Xq24 resulting in a triad of skeletal myopathy, hypertrophic cardiomyopathy, and mild mental retardation.[2] XMEA, also known as X-linked vacuolated myopathy,[6] is slowly progressive, with no other organ involvement. Linkage analysis identified the XMEA locus in the most telomeric region of chromosome X.[7] Infantile AVM patients were floppy at birth, with myopathy and cardiomyopathy causing early death.[4] Recently, a patient with adult-onset AVM with multiorgan involvement (eyes, heart, liver, lung, kidney, and skeletal muscles) was reported. In this study, we describe a new Chinese-American family with a severe form of myopathy with AVSF.

From the Department of Neuromuscular Research (Drs. Yan, Tanaka, Sugie, Noguchi, Nonaka, Hayashi, and Nishino), National Institute of Neuroscience, National Hospital for Mental, Nervous and Muscular Disorders (Drs. Nobutoki and Nonaka), National Center of Neurology and Psychiatry, Kodaira, Tokyo; Dr. Woo's Pediatric Clinic (Dr. Woo), Kyoto; Departments of Neurology (Dr. Murase) and Pediatrics (Dr. Higuchi), National Hospital Organization Utano National Hospital, Kyoto, Japan; and Department of Neurology (Dr. Yan), Qilu Hospital of Shandong University, Jinan, China.

Supported partly by the Research on Health Sciences focusing on Drug Innovation and the Research on Psychiatric and Neurologic Diseases and Mental Health from the Japanese Health Sciences Foundation; partly by a Grant-in-Aid for Scientific Research from the Japan Society for the Promotion of Science; and partly by a Research Grant (17A-10) for Nervous and Mental Disorders from the Ministry of Health, Labor and Welfare.

Disclosure: The authors report no conflicts of interest.

Received February 17, 2005. Accepted in final form June 20, 2005.

Address correspondence and reprint requests to Dr. Ichizo Nishino, Department of Neuromuscular Research, National Institute of Neuroscience, National Center of Neurology and Psychiatry, 4-1-1 Ogawa-Higashi, Kodaira, Tokyo 187-8502, Japan; e-mail: nishino@ncnp.go.jp

Methods. All clinical materials used were obtained with informed consent. Genomic DNA was isolated from peripheral lymphocytes using a standard technique. Muscle specimens were flash-frozen in isopentane chilled with liquid nitrogen for histologic analysis or fixed in 2% glutaraldehyde and postfixed in osmium tetroxide for electron microscopic analysis.

Seven male patients in this family presented with similar clinical symptoms (figure 1). Patient IV-2 (figure 1, C and D), a 7-year-old boy from nonconsanguineous Chinese-American parents, had congenital hypotonia and hypoventilation requiring respiratory support for 3 days. Because of difficulty suckling and dysphagia, nasogastric tube feeding was initiated until age 2½ years. The patient's motor milestones were delayed, with sitting at 9 months and walking with support at 2 years. Thereafter, his motor development deteriorated, with progressive muscle weakness and crawling at age 7 years. His serum creatine kinase (CK) level was increased at 1,962 IU/L (reference range = 51 to 197). Generalized muscle atrophy and weakness, including facial and neck muscles, were observed. He had a high-arched palate with normal mentation. EKG revealed incomplete right bundle-branch block, and echocardiography showed left ventricular hypertrophy. Needle EMG of the right biceps brachii revealed complex repetitive discharges without fibrillation potentials or positive sharp waves and low-amplitude, short-duration motor unit potentials with early recruitment, which are compatible with a chronic myopathic condition.

Patient IV-1 (figure 1, B and D) was the 9-year-old elder brother of the proband. He was also hypotonic at birth, with an increased CK level (2,000 IU/L). He also required nasogastric tube feeding until age 2 years. He sat at 8 months and walked at 21 months but became wheelchair bound at age 5 years. He had generalized muscle weakness and atrophy, including facial and neck muscles, with no cardiac or CNS involvement.

Two maternal uncles (III-2 and -3) had asphyxia and died immediately after birth. Another maternal uncle (III-5) had a weak cry and died at age 8 months. Two maternal grandmother's brothers (II-3 and -4) died within several months after birth because of difficulty suckling. No female relatives had clinical signs of myopathy, including the mother (III-4) of the index patients, with a normal CK level (39 IU/L).

Haplotyping and linkage analysis. Haplotype analysis of the genomic DNA from two affected (IV-1 and IV-2) and six unaffected family members (I-2, II-1, II-2, III-1, III-4 and III-6) (see figure 1) was performed using an ABI PRISM 310 genetic analyzer (PE Applied Biosystems, CA) with the following 23 microsatellite markers on chromosome X: Xpter-DXS1060-DXS8051-DXS987-DXS1226-DXS121-DXS1068-DXS993-DXS991-DXS986-DXS990-DXS458-DXS1106-DXS8096-DXS8055-DXS1001-DXS1047-DXS691-DXS1227-DXS8043-DXS1215-DXS8091-DXS8069-DXS1073-Xqter. The multipoint linkage analysis from the haplotype data were conducted using GENEHUNTER.[8]

Sequence analysis. Mutation analysis of LAMP-2 was performed in two affected patients (IV-1 and IV-2) using an ABI PRISM 3100 automated sequencer (PE Applied Biosystems), as described.[2]

 Copyright © 2005 by AAN Enterprises, Inc.
Downloaded from www.neurology.org by LISA TIANO on February 6, 2006

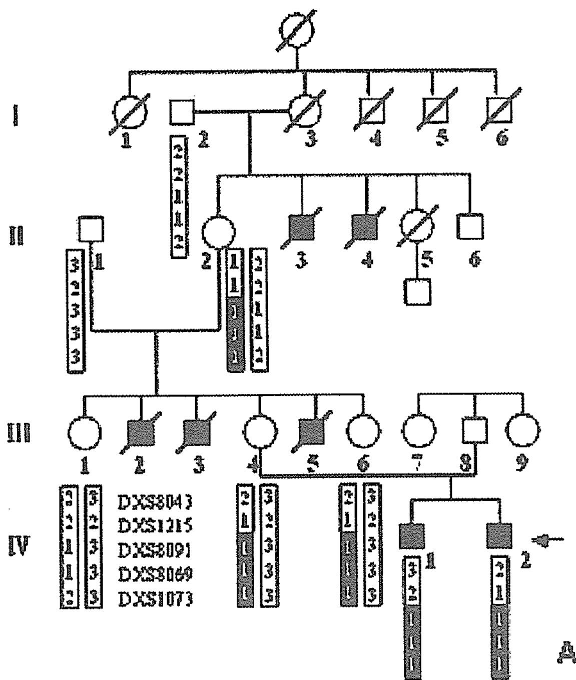

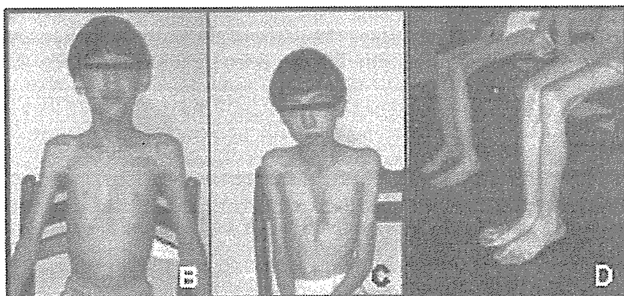

Figure 1. In the pedigree of the family (A), shaded boxes are the affected members. Symbols with diagonal lines represent deceased individuals. In the haplotype chart of this family, only informative regions (Xq27.2 to Xqter) are presented. The most important candidate region containing a common haplotype in three generations is highlighted by shaded boxes. Patient IV-2 (B and D) and Patient IV-1 (C and D) showed facial and neck muscle involvement, thoracic cage deformity, and severe generalized muscle atrophy.

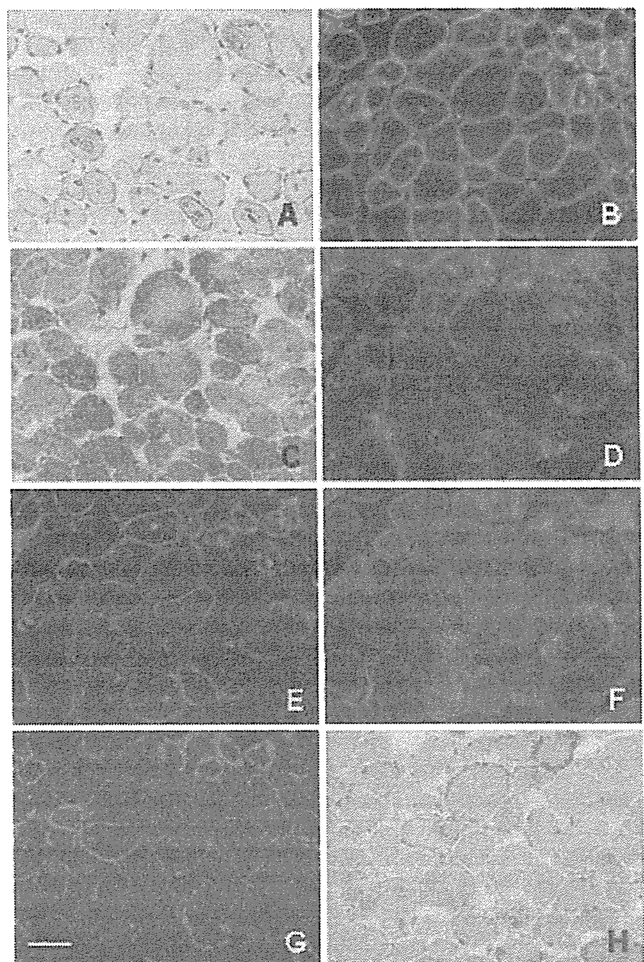

Figure 2. Muscle pathologic features (Patient IV-2). The vacuolar membranes have increased acetylcholinesterase (AChE) activities (A), and dystrophin is expressed in most intrasarcoplasmic vacuolar membranes (B). Strong acid phosphatase activity is observed inside vacuoles (C). Increased immunoreactivity of LAMP-2 is seen both at the surface membranes and within the cytoplasm of affected fibers (D). LIMP-1/CD63 is strongly stained at the sarcolemma and within the cytoplasm (E), and some cytoplasmic granular staining is colocalized with LC3 (F). Marked C5-9 membrane attack complex deposition is seen at the sarcolemma of almost all muscle fibers (G). By alizarin red, calcium deposition is seen at the sarcolemma and occasionally within the cytoplasm (H). Bar = 30 μm.

Histochemical and immunohistochemical analyses and electron microscopic studies. Serial frozen sections were stained with a battery of histochemical methods including hematoxylin and eosin (H-E), modified Gomori-trichrome, acid phosphatase, AChE, nonspecific esterase (NSE), periodic acid–Schiff, and alizarin red.

Immunohistochemical analysis was done using antibodies for LAMP-2 (H4B4; Developmental Studies Hybridoma Bank [DSHB]), LIMP-1/CD63 (H5C6; DSHB), dystrophin (NCL-DYS1; Novocastra Laboratories), C5b-9 membrane attack complex (MAC; DAKO Co.), microtubule-associated protein 1 light chain (LC3; kindly provided by Dr. Ueno[9]), CD59 (Biogenesis, Ltd.), dystrophin (NCL-DYS2; Novocastra), dysferlin (NCL-Hamlet 2; Novocastra), alpha sarcoglycan (Novocastra), caveolin-3 (Transduction Laboratories), and merosin (Chemicon International).

Electron microscopy was performed using a Hitachi H-7100 electron microscope.

Results. The skeletal muscle from patient IV-2 showed marked variation in fiber size with endomysial fibrosis. There are many intracytoplasmic vacuoles with activity for NSE (data not shown) and AChE (figure 2, A). Positive immunoreaction was observed at the vacuolar membranes with all five antibodies for sarcolemmal and extracellular matrix protein including dystrophin (figure 2, B). Within vacuoles, strong acid phosphatase activity was seen (figure 2, C), and vacuolar membranes showed LAMP-2 staining (figure 2, D), indicating the lysosomal nature of the vacuoles. Strong immunoreaction to LIMP-1/CD63, a lysosomal membrane protein, was observed both at the sarcolemma and inside the vacuoles (figure 2, E). LC3, having a crucial role for autophagosome formation,[9] was abundant in the cytoplasm, and some colocalized with LIMP-1/CD63 (figure

Downloaded from www.neurology.org by LISA TIANO on February 6, 2006

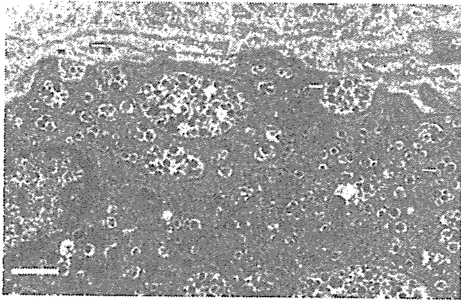

Figure 3. Electron microscopy shows large accumulation of dense globes and amorphous granules surrounded by a single layer membrane under sarcolemma or between the multiple layered basal lamina (white arrows). Some of these dense globes are encircled by a double-layered membrane (arrows). Some vacuoles are attached to the sarcolemma indicating exocytotic process. Bar = 1 μm.

2, F). MAC (figure 2, G) and calcium (figure 2, H) were markedly deposited at the sarcolemma in most fibers. CD59, an inhibitor of MAC, was positive in all muscle fibers, including MAC-positive ones (data not shown). Muscles from patients with Danon disease did not stain for LAMP-2. Membrane staining of LIMP-1/CD63 was weak, and MAC deposition was rarely observed (data not shown).

Electron microscopy of the patients' muscles revealed that numerous electron dense granules accumulated in various sizes of intracytoplasmic vacuoles (figure 3). Some larger granules were surrounded by double-layered membrane. The severely affected muscle fibers were surrounded by multilayered basal lamina wherein dense granules were also observed.

Mapping of the disease in this family using polymorphic microsatellite markers spanning the entire X-chromosome showed the highest multipoint lod score peak of 0.46 between markers DXS8069 and DXS1073. Other X chromosome region showed negative lod score, except for the small regions around DXS1226 (maximum 0.14) and DXS458 (maximum 0.08), suggesting that the causative gene may be localized in Xq28 (distal to DXS1215) (figure 1, A).

No mutation in *LAMP-2* was identified in the two affected patients examined.

Discussion. XMEA is clinically characterized as slowly progressive or nonprogressive myopathy with AVSF. The onset of symptoms usually ranges between ages 5 and 10 years, presenting with difficulty in climbing stairs and running without loss of ambulation. Lifespan is not altered. In contrast, our patients have more severe clinical manifestations with infantile hypotonia, dyspnea, and dysphagia. Some of the relatives died in early infancy, probably because of the same disease. Nevertheless, the pathologic features of our patients—multilayered basal lamina and intense sarcolemmal deposition of MAC and calcium in addition to AVSF—have been described as pathognomonic of XMEA.[6,10] In fact, the disease is pathologically indistinguishable from XMEA, suggesting allelism to XMEA. This notion is supported by the facts that the disease is transmitted through an X-linked recessive inheritance pattern and that haplotype analysis suggested Xq28, the chromosomal region for XMEA,[7] as a possible locus of this disease. The low lod score is due to small family size. Furthermore, similar pathologic findings were also reported in infantile AVM,[4] suggesting that it may also be allelic to XMEA. The identification of the XMEA gene will resolve the issue of allelism of these disorders to XMEA.

Although the genetic cause is still unknown, colocalization of LC3 and LIMP-1/CD63 in the patients' muscles, together with numerous dense granules on electron microscopy, suggests abnormal protein degradation as part of the pathomechanism in infantile AVSF as well as in XMEA.

Acknowledgment

The authors thank the patients and their families for their cooperation, Dr. Takashi Ueno (Jutendo University, Tokyo, Japan) for providing the LC3 antibody, Dr. Michio Hirano (Columbia University, New York, NY) for reviewing the manuscript, Dr. Jun Kimura (University of Iowa, Iowa City, IA) for comments on EMG findings, and Dr. Mina Astejada (National Center of Neurology and Psychiatry, Kodaira, Tokyo, Japan) for comments on the manuscript.

References

1. Sugie K, Noguchi S, Kozuka Y, et al. Autophagic vacuoles with sarcolemmal features delineate Danon disease and related myopathies. J Neuropathol Exp Neurol 2005;64:513–522.
2. Nishino I, Fu J, Tanji K, et al. Primary LAMP-2 deficiency causes X-linked vacuolar cardiomyopathy and myopathy (Danon disease). Nature 2000;406:906–910.
3. Saviranta P, Lindlof M, Lehesjoki AE, et al. Linkage studies in a new X-linked myopathy, suggesting exclusion of DMD locus and tentative assignment to distal Xq. Am J Hum Genet 1988;42:84–88.
4. Yamamoto A, Morisawa Y, Verloes A, et al. Infantile autophagic vacuolar myopathy is distinct from Danon disease. Neurology 2001;57:903–905.
5. Kaneda D, Sugie K, Yamamoto A, et al. A novel form of autophagic vacuolar myopathy with late-onset and multi-organ involvement. Neurology 2003;61:128–131.
6. Villanova M, Louboutin JP, Chateau D, et al. X-linked vacuolated myopathy: complement membrane attack complex on surface membrane injured muscle fibers. Ann Neurol 1995;37:637–645.
7. Minassian BA, Aiyar R, Alic S, et al. Narrowing in on the causative defect of an intriguing X-linked myopathy with excessive autophagy. Neurology 2002;59:596–601.
8. Kruglyak L, Daly MJ, Reeve-Daly MP, Lander ES. Parametric and nonparametric linkage analysis: a unified multipoint approach. Am J Hum Genet 1996;58:1347–1363.
9. Anasuma K, Tanida I, Shirato I, et al. MAP-LC3, a promising autophagosomal marker, is processed during the differentiation and recovery of podocytes from PAN nephrosis. FASEB J 2003;17:1165–1167.
10. Louboutin JP, Villanova M, Lucas-Heron B, Fardeau M. X-linked vacuolated myopathy: membrane attack complex deposition on muscle fiber membranes with calcium accumulation on sarcolemma. Ann Neurol 1997;41:117–120.

Downloaded from www.neurology.org by LISA TIANO on February 6, 2006

A new congenital form of X-linked autophagic vacuolar myopathy

C. Yan, M. Tanaka, K. Sugie, T. Nobutoki, M. Woo, N. Murase, Y. Higuchi, S. Noguchi, I. Nonaka, Y. K. Hayashi and I. Nishino

Neurology 2005;65;1132-1134
DOI: 10.1212/01.wnl.0000178979.19887.f5

This information is current as of February 6, 2006

Updated Information & Services	including high-resolution figures, can be found at: http://www.neurology.org/cgi/content/full/65/7/1132
Subspecialty Collections	This article, along with others on similar topics, appears in the following collection(s): **Muscle disease** http://www.neurology.org/cgi/collection/muscle_disease
Permissions & Licensing	Information about reproducing this article in parts (figures, tables) or in its entirety can be found online at: http://www.neurology.org/misc/Permissions.shtml
Reprints	Information about ordering reprints can be found online: http://www.neurology.org/misc/reprints.shtml

Downloaded from www.neurology.org **by LISA TIANO on February 6, 2006**

J Neuropathol Exp Neurol
Copyright © 2005 by the American Association of Neuropathologists, Inc.

Vol. 64, No. 6
June 2005
pp. 513–522

ORIGINAL ARTICLE

Autophagic Vacuoles with Sarcolemmal Features Delineate Danon Disease and Related Myopathies

Kazuma Sugie, MD, PhD, Satoru Noguchi, PhD, Yoshimichi Kozuka, PhD, Eri Arikawa-Hirasawa, MD, PhD, Mikihito Tanaka, PhD, Chuanzhu Yan, MD, Paul Saftig, PhD, Kurt von Figura, PhD, Michio Hirano, MD, Satoshi Ueno, MD, PhD, Ikuya Nonaka, MD, PhD, and Ichizo Nishino, MD, PhD

Abstract

Among the autophagic vacuolar myopathies (AVMs), a subgroup is characterized pathologically by unusual autophagic vacuoles with sarcolemmal features (AVSF) and includes Danon disease and X-linked myopathy with excessive autophagy. The diagnostic importance and detailed morphologic features of AVSF in different AVMs have not been well established, and the mechanism of AVSF formation is not known. To address these issues, we have performed detailed histologic studies of myopathies with AVSF and other AVMs. In Danon disease and related AVMs, at the light microscopic level, autophagic vacuoles appeared to be accumulations of lysosomes, which, by electron microscopy consisted of clusters of autophagic vacuoles, indicative of autolysosomes. Some autolysosomes were surrounded by membranes with sarcolemmal proteins, acetylcholinesterase activity, and basal lamina. In Danon disease, the number of fibers with AVSF increased linearly with age while the number with autolysosomal accumulations decreased slightly, suggesting that AVSF are produced secondarily in response to autolysosomes. Most of the AVSF form enclosed spaces, indicating that the vacuolar membranes may be formed in situ rather than through sarcolemmal indentation. This unique intracytoplasmic membrane structure was not found in other AVMs. In conclusion, AVSF with acetylcholinesterase activity are autolysosomes surrounded by secondarily generated intracytoplasmic sarcolemma-like structure and delineates a subgroup of AVMs.

Key Words: Autophagic vacuole, Autophagy, Danon disease, LAMP-2, Lysosome.

From the Departments of Neuromuscular Research (KS, SN, MT, CY, I Nishino) and Ultrastructural Research (YK), National Institute of Neuroscience, National Hospital for Mental (I Nonaka, I Nishino), Nervous and Muscular Disorders, National Center of Neurology and Psychiatry, Kodaira, Tokyo, Japan; the Department of Neurology (KS, SU), Nara Medical University, Kashihara, Nara, Japan; the Department of Neurology (EA-H), Juntendo University School of Medicine, Tokyo, Japan; the Department of Biochemistry (PS), University of Kiel, Kiel, Germany; Zentrum Biochemie und Moleculare Zellbiologie (PS, KvF), Abteilung Biochemie II, Universität Göttingen, Göttingen, Germany; and the Department of Neurology (MH), Columbia University, New York, New York.

Send correspondence and reprint requests to: Ichizo Nishino, MD, PhD, Department of Neuromuscular Research, National Institute of Neuroscience, National Center of Neurology and Psychiatry (NCNP), 4-1-1 Ogawahigashi-cho, Kodaira, Tokyo 187-8502, Japan; E-mail: nishino@ncnp.go.jp

INTRODUCTION

Danon disease, an X-linked vacuolar cardiomyopathy and myopathy, is caused by primary deficiency of lysosome-associated membrane protein-2 (LAMP-2), a major lysosomal membrane protein (1–4). Muscle biopsies contain small autophagic vacuoles with cytoplasmic debris. The membranes of these vacuoles have structural features of sarcolemma and biochemical activities of acetylcholinesterase (AChE) and nonspecific esterase (NSE) (5). Although some sarcolemmal proteins, including dystrophin, have been detected in vacuolar membranes (3), the presence of other sarcolemmal proteins has not been studied. In addition, the pathomechanism by which LAMP-2 deficiency leads to the formation of these peculiar autophagic vacuoles with sarcolemmal features (AVSFs) is still unknown.

AVSFs are also seen in X-linked myopathy with excessive autophagy (XMEA) (6), infantile autophagic vacuolar myopathy (AVM) (7), and adult-onset AVM with multiorgan involvement (8). XMEA is clinically characterized by a mild pure skeletal myopathy. In contrast, infantile AVM involves both cardiac and skeletal muscles and patients die within several months after birth, whereas adult-onset AVM affects multiple organs including liver, kidney, and skeletal muscles. All of these diseases show multilayered basal lamina and the deposition of C5b-9 over the surface of the muscle fiber; these features are not seen in Danon disease. Nevertheless, these diseases are likely to share a common pathomechanism since they also have AVSF similar to those seen in Danon disease (9).

To delineate subtypes of AVMs and to gain insights into their pathomechanisms, we have performed detailed histologic evaluations of muscle from patients with Danon disease, XMEA, infantile AVM, and adult-onset AVM, and from LAMP-2 deficient mice (10, 11). Moreover, to evaluate the specificity of the AVSF we have also characterized autophagic vacuoles in other lysosomal myopathies, including acid maltase deficiency (AMD), sporadic inclusion body myositis (SIBM), and distal myopathy with rimmed vacuoles (DMRV), which has recently been shown to be the same disease as hereditary inclusion body myopathy (HIBM).

MATERIALS AND METHODS

Patients

We examined skeletal muscles of ten affected men from 8 families with genetically confirmed Danon disease. We also